https://doi.org/10.5194/bg-2022-14
Preprint. Discussion started: 14 February 2022

Biogeosciences Discussions

Assessing the spatial and temporal variability of MeHg biogeochemistry and bioaccumulation in the Mediterranean Sea with a coupled 3D model

Ginevra Rosati[1], Donata Canu[1], Paolo Lazzari[1], Cosimo Solidoro[1]

[1] National Institute of Oceanography and Applied Geophysics - OGS

Correspondence to: Ginevra Rosati (grosati@inogs.it)

Abstract. Human exposure to mercury (Hg) is a cause of concern, due to the biomagnification of the neurotoxic species monomethylmercury (MMHg) in marine ecosystems. Previous research revealed that commercial fish species in the Mediterranean Sea ecosystems are particularly enriched in Hg, due to a combination of physical and ecological factors. Since the fate of Hg depends on the interactions among several biogeochemical and physical drivers, biogeochemical modelling is crucial to support the integration and interpretation of field data. Here, we develop and apply a coupled transport-biogeochemical-metal bioaccumulation numerical model (OGSTM-BFM-Hg), to simulate the biogeochemical cycling of the main Hg species (Hg^{II}, Hg^{0}, MMHg, and DMHg) in seawater, organic detritus, and through the planktonic food web. The model is applied to a 3D domain of the Mediterranean Sea to investigate the spatial and temporal variability of MeHg distribution and bioaccumulation. Model results reproduce the strong vertical and zonal gradients of MeHg concentrations related to primary production consistently with the observations, and highlight the role of winter deep convection and summer water stratification in shaping the MeHg vertical distribution, including sub-surface MeHg maximum. The modelled bioaccumulation dynamics in plankton food webs are characterized by a high spatial and temporal variability that is driven by plankton phenology, and are in agreement with available field data of concentrations in plankton and with other indicators, such as bioconcentration factors (BCFs) and trophic magnification factors (TMFs). Model results pointed out that the increment in water temperature linked to a decline of deep convection can cause an increase in water MeHg concentrations with cascading effects on plankton exposure and bioaccumulation.

1 Introduction

The anthropogenic alteration of mercury (Hg) biogeochemical cycle has led to global enrichment of Hg concentrations in all the environmental compartments (Amos et al., 2015; UNEP, 2019; Zhang et al., 2014a, 2014b) and concerns over human exposure to neurotoxic monomethylmercury (MMHg), which is produced in the ocean and biomagnifies in marine food webs (UNEP, 2019). The ocean has absorbed 50% of anthropogenic Hg historical emissions, 35% of which currently stored in the water and the rest in the sediments (Zhang et al., 2014b): relative to pre-anthropogenic levels, the Hg enrichment is 230% in surface ocean waters, 25% in intermediate waters, and 12% in deep waters (UN Environment 2019).

https://doi.org/10.5194/bg-2022-14
Preprint. Discussion started: 14 February 2022


Biogeosciences Discussions Open Access EGU

Models and observations (Lamborg et al., 2014; Zhang et al., 2014b) suggest that the oceanic water column contains 280-370 Mmol of anthropogenic Hg (equivalent to about 70000 tons), a large part of which is recycled within surface and intermediate water due to the biological carbon pump and the microbial loop (e.g. Zhang et al., 2018). Hg is scavenged from surface water by organic particles through adsorption and uptake, transported downward via particles sinking, and released in the dissolved phase following particles degradation. The locally-increased microbial activity and availability of inorganic Hg at the depth of particles remineralization are also thought to promote Hg methylation (Cossa et al., 2009; Heimbürger et al., 2010; Sunderland et al., 2009). Concurrent biological and photochemical transformations occur in the water column driving the interconversions among the main mercury species in seawater (inorganic Hg [Hg^{II}], methylmercury [MMHg], elemental Hg [Hg^{0}] and dimethylmercury [DMHg]). The resulting vertical distribution of Hg species mirrors the local equilibrium among a number of biogeochemical and physical drivers. However, recent comprehensive reviews of the current understanding of Hg fate in the ocean highlighted still a high uncertainty in describing and quantifying most of these processes (Bowman et al., 2020; Mason et al., 2012; Sonke et al., 2013).

MeHg (defined as the sum of MMHg and DMHg) is more frequently measured than the individual methylated species. In oceanic and Mediterranean areas with high primary production the MeHg vertical distribution is characterized by low concentrations at surface due to photo-degradation and concentrations maxima coincident with the maximum in apparent oxygen utilization, a proxy for heterotrophic activity (Cossa et al., 2009; Sunderland et al., 2009). These observations suggest that most oceanic MeHg is produced in situ. This conclusion is also supported by estimates of MeHg fluxes in the ocean (Mason et al., 2012; Zhang et al., 2020) and by studies based on stable Hg isotopes (Blum et al., 2013; Motta et al., 2019). The role of DMHg in controlling MMHg dynamics remains puzzling: recent observations (Cossa et al., 2017) from the North Western Mediterranean Sea support the idea that DMHg is produced from Hg^{II} in highly productive waters and then degraded to MMHg (Conaway et al., 2009), however only an abiotic pathway has been directly identified for the formation of DMHg (Jonsson et al., 2016) and rates of DMHg formation from Hg^{II} measured in polar water were negligible compared to methylation rates from Hg^{II} to MMHg (Lehnherr et al., 2011).

Tunas and other commercial fish species from the Mediterranean Sea are particularly enriched in Hg compared to the same species from other geographical areas (Cossa et al., 2012; Cossa and Coquery, 2005; Harmelin-Vivien et al., 2009; Tseng et al., 2021). It has been suggested that, along with other ecological features of the whole food web, this is due to a shallower occurrence of the MeHg concentrations maxima compared to the Ocean that results in higher phytoplankton exposure and bioaccumulation (Cossa et al., 2012). Available observations on MeHg distribution in the Mediterrenan Sea, suggest that concentrations are lower in the oligotrophic waters of the Ionian Sea than in the mesotrophic waters of the Northwestern Mediterranean (Cossa et al., 2009) and Adriatic Sea (Kotnik et al., 2015).

Recent efforts to couple the dynamics of biological carbon pump and microbial loop with Hg dynamics, including bioaccumulation in the lower food web provided global-scale assessments of MeHg production and bioaccumulation (Wu et al., 2021, 2020; Zhang et al., 2020). The only study modelling the Hg dynamics in the Mediterranean Sea (Žagar et al., 2007) did not include any biological component. Much of the current knowledge on the dynamics of MeHg in the open sea has been

https://doi.org/10.5194/bg-2022-14
Preprint. Discussion started: 14 February 2022

acquired only afterwards (Bowman et al., 2016, 2015; Cossa et al., 2017, 2009; Heimbürger et al., 2010; Lehnherr et al., 2011; Monperrus et al., 2007; Munson et al., 2018, 2015; Ortiz et al., 2015; Sunderland et al., 2009).

Here, we couple a model for Hg biogeochemistry (Canu et al., 2019; Rosati et al., 2020, 2018; Zhang et al., 2020) with the 3D transport biogeochemical model OGSTM-BFM (Lazzari et al., 2021, 2010; Salon et al., 2019) to investigate spatial and temporal variability of MeHg dynamics in the Mediterranean Sea. The coupled model (Fig. 1), which has a 1/16° horizontal resolution, describes the biotic and abiotic interconversions among four Hg species (Hg^{II}, MMHg, Hg^0, and DMHg), as well as other key processes of Hg cycle such as partitioning to detritus, sinking to the seabed, exchange of gaseous Hg with the atmosphere, and bioaccumulation in 4 phyto- and 4 zooplankton functional groups (Lazzari et al., 2012; Vichi et al., 2015). The agreement with observations has been improved by tuning the sinking velocity of organic detritus and by exploring the sensitivity to alternative parameterizations of Hg methylation. Model results are compared to available observations discussing the implications of spatial and temporal variability of modelled MeHg distributions in water and plankton.

2 Methods

The Biogeochemical Flux Model BFM (Vichi et al., 2015) is a model that describes the cycling of Carbon, Nitrogen Phosphorus, and Silica through dissolved, living and non-living particulate phases of the marine environment. The description of the planktonic food web is based on the plankton functional type (PFT) approach: the pool of species having similar traits (nutrients affinities, light affinity, prey-predator relationships) are described by the same variable. In the BFM, PFTs have variable stoichiometry, and simulate the lower trophic levels of marine food webs up to carnivorous zooplankton (Sect. 2.1). The OGSTM-BFM model has been coupled off-line to the ocean general circulation model (NEMO) to investigate different issues related to the Mediterranean biogeochemistry (Canu et al., 2015; Cossarini et al., 2021, 2015; Lazzari et al., 2021, 2016, 2014, 2012) and it is now routinely used as the backbone of the biogeochemical component of the Copernicus CMEMS Mediterranean system (https://resources.marine.copernicus.eu/products, (Salon et al., 2019; Terzić et al., 2019). The integration of a Hg cycling module in the BFM-OGSTM model adds more flexibility to this system and open the way to novel operational oceanography applications. Here the OGSTM-BFM-Hg model is implemented (Fig. 1), by coupling the OGSTM-BFM model with the equations describing mercury (Hg) species partitioning, transformation, transport (Sect. 2.2), bioconcentration in phytoplankton (Sect. 2.3), and trophic transfer to zooplankton (Sect. 2.4). The coupled model is used to investigate the Hg cycling and bioaccumulation dynamics (Sect. 2.5) at the base of the Mediterranean Sea food webs. The model has a 1/16° horizontal resolution (approximately 6 km) and 72 vertical levels and runs with a 300 seconds time step. A model spin-up of 13 years forced with climatological data (Sect. 2.6) is performed, and the results of last year of simulation (2017) are analysed.

https://doi.org/10.5194/bg-2022-14
Preprint. Discussion started: 14 February 2022

2.1 BFM model dynamics

The BFM model dynamically simulates 9 plankton functional types (PFTs) representative of 4 phytoplankton groups (picophytoplankton, nanophytoflagellates, diatoms, and large phytoplankton), 4 zooplankton groups (eterotrophic nanoflagellates, microzooplankton, omnivorous mesozooplankton, and carnivorous mesozooplankton), and 1 group of heterotrophic bacteria (Vichi et al. 2015). The model reproduces the fluxes of carbon, nitrogen, phosphorous, and silicates from the inorganic nutrients pool to organisms (phytoplankton, zooplankton and bacteria) and organic compounds pools (particulate and dissolved organic carbon, POC and DOC) with a variable stoichiometric formulation. Non-living organic matter includes one class of organic detritus (POC) and three classes of DOC (labile, semi-labile, and semi-refractory).

2.2 Biogeochemical dynamics in the Hg model

The Hg biogeochemical model (Canu and Rosati, 2017; Canu et al., 2019; Melaku Canu et al., 2015; Rosati et al., 2020, 2018, in prep., Zhang et al., 2020) simulates the cycling of four mercury species in marine water (Fig. 2): inorganic divalent Hg (Hg^{II}), monomethylmercury (MMHg), elemental mercury (Hg^0), and dimethylmercury (DMHg). Eq. (1-4) describe the time variation of non-conservative tracers representing Hg species, omitting advective and diffusive processes that are resolved by the transport model.

$$\frac{d\,Hg^{II}}{dt} = -k_{met}\{Hg^{II}\} + k_{demet}\{MMHg\} - k_{phred}\{Hg^{II}_{DOC} + HgCl_n\} + k_{phox}\{Hg^0\} - k_{biored}\{Hg^{II}_{DOC} + HgCl_n\} + k_{biox}\{Hg^0\} + (1-\alpha)\,k_{phdm}\{MMHg_{DOC} + MeHgCl\} - \omega_s\{Hg^{II}_{POC}\} \quad (1)$$

$$\frac{d\,MMHg}{dt} = k_{met}\,Hg^{II} - k_{demet}\,MMHg - k_{phdm}\{MMHg_{DOC} + MMHgCl\} - k_{met}\{MMHg\} + k_{phdm2}\,DMHg - \omega_s\{MMHg_{POC}\} - \frac{d\,MMHg_{phy}}{dt} + Ex_{zoo}\frac{MMHg_{zoo}}{C_{zoo}} + D_{zoo}\frac{MMHg_{zoo}}{C_{zoo}} \quad (2)$$

$$\frac{d\,Hg^0}{dt} = +k_{phred}\{Hg^{II}_{DOC} + HgCl_n\} - k_{phox}\{Hg^0\} + k_{biored}\{Hg^{II}_{DOC} + HgCl_n\} - k_{biox}\{Hg^0\} + \alpha\,k_{phdm}\{MMHg_{DOC} + MMHgCl\} - k_{vol}\left\{Hg^0_w - \frac{Hg^0_{atm}}{K_{H'}}\right\} \quad (3)$$

$$\frac{dDMHg}{dt} = +k_{met}\{MMHg\} - k_{phdm2}\{DMHg\} \quad (4)$$

Desorption rates of Hg from particles in the ocean are negligible, and dynamics of Hg between the particulate and the dissolved phase can be synthetized as a balance between adsorption from the dissolved phase and particle remineralization (Lamborg et al., 2016). Accordingly, in the model the partitioning of Hg^{II} and MMHg between particulate species (Hg^{II}_{POC}, $MMHg_{POC}$, associated to organic detritus) and dissolved species (Hg^{II}_{DOC}, $MMHg_{DOC}$, associated to dissolved organic carbon, and ionic species $HgCl_n$ and $MMHgCl$) is calculated assuming repartition at thermodynamic equilibrium, taking into account dynamic POC remineralization and sinking based on the biogeochemical processes simulated in the BFM model (Fig.s 1 and 2). The

https://doi.org/10.5194/bg-2022-14
Preprint. Discussion started: 14 February 2022


Biogeosciences Discussions Open Access EGU

fraction of each Hg species with respect to its total ($f_{Hg\text{-}POC}$, $f_{Hg\text{-}DOC}$, f_{HgCl}, $f_{MeHg\text{-}POC}$, $f_{MeHg\text{-}DOC}$, f_{MegCl}) is computed (e.g., Eq. 5-7 for Hg^{II}) from partition coefficients K_D (Choe et al., 2003; Choe and Gill, 2003; Lamborg et al., 2016) that are set as model parameters (Tab. S1), and from DOC and POC concentrations. Then, concentrations of particulate and dissolved species of Hg^{II} and MMHg are calculated from the corresponding fraction and the total concentration of the state variable (e.g., Eq. 8). The pool of dissolved gaseous mercury species (DGM, i.e., Hg^0 and DMHg) is assumed to be entirely in the dissolved phase.

$$f_{Hg_{POC}} = \frac{Hg^{II}_{POC}}{Hg^{II}_{TOT}} = \frac{POC\ K_{D\ Hg\text{-}POC}}{1+DOC\ K_{D\ Hg\text{-}DOC}+\ POC\ \ K_{D\ Hg\text{-}POC}} \quad (5)$$

$$f_{Hg_{DOC}} = \frac{Hg^{II}_{DOC}}{Hg^{II}_{TOT}} = \frac{DOC\ K_{D\ Hg\text{-}POC}}{1+DOC\ K_{D\ Hg\text{-}DOC}+\ POM\ \ K_{D\ Hg\text{-}POC}} \quad (6)$$

$$f_{HgCl} = \frac{HgCl_n}{Hg^{II}_{TOT}} = \frac{1}{1+DOC\ K_{D\ Hg\text{-}DOC}+POM\ \ K_{D\ Hg\text{-}POC}} \quad (7)$$

$$Hg^{II}_{POC} = f_{Hg_{POC}}\ Hg^{II}_{TOT} \quad (8)$$

Once the partitioning is determined, the model computes the transformations fluxes based on first order rates (k_x, d^{-1} Tab. S2), the bioconcentration (Sect. 2.3) and bioaccumulation fluxes (Sect. 2.4), the sinking of Hg_{POC} and $MMHg_{POC}$, the advective transport within the model domain and at the model boundaries (i.e. Gibraltar Strait), and the exchange of Hg^0 with the atmosphere. Microbial Hg methylation ($k_{met}\ Hg^{II}$), reduction ($k_{biored}\ \{Hg^{II}_{DOC}\ +HgCl_n\}$), and oxidation ($k_{biox}\ Hg^0$) are parameterized as functions of particulate organic matter remineralization (Zhang et al., 2020, 2014a), which is read from the BFM model. The direct conversion of Hg^{II} to DMHg is assumed to be negligible, due to the low rates observed in the only dataset available for this process (Lehnherr et al., 2011). Although several observations linked Hg methylation to oxygen consumption and organic matter remineralization in the water column, a full mechanistic understanding of methylation and demethylation is still lacking (An et al., 2019; Wang et al., 2020). Here we assumed that both reactions involve the entire Hg^{II} and MMHg pools (Ortiz et al., 2015; Schaefer and Morel, 2009; Zhang et al., 2019). Photochemical transformations, i.e. photoreduction ($k_{phred}\ \{Hg^{II}_{DOC}\ +HgCl_n\}$), photooxidation ($k_{phox}\ Hg^0$), and photodegradation of MMHg ($k_{phdem}\ \{MMHg_{DOC}\ +MMHgCl\}$) and DMHg ($k_{phdm2}\ DMHg$) are assumed to act only on the dissolved fractions, and are a function of the attenuated shortwave flux (Zhang et al., 2014a). MMHg photodegradation is assumed to yield both Hg^0 and Hg^{II} ($k_{phdm}\ \{MMHg_{DOC}+MeHgCl\}$) due to the contrasting results in experimental studies (Luo et al., 2020).

The gas-exchange flux of Hg^0 with the atmosphere ($k_{vol}\ \{Hg^0_w - Hg^0_{atm}/K_{H'}\}$) is using the Nightingale's parameterization (Nightingale et al., 2000) for the rate constant k_{vol}, (Eq. (9)), which depends on wind speed (u_{10}, m/s) and on the ratio of Hg Schmidt number to CO_2 Schmidt number ($ScHg_w/ScCO_{2_w}$).

$$k_{vol} = \left(0.222u^2_{10} + 0.333u_{10}\right)\left(\frac{ScHg_w}{ScCO_{2_w}}\right)^{-0.5} \quad (9)$$

https://doi.org/10.5194/bg-2022-14
Preprint. Discussion started: 14 February 2022

Current knowledge on dynamics and concentrations of DMHg in the ocean and in the atmosphere does not allow a detailed modelling representation (Baya et al., 2015; Coale et al., 2018; De Simone et al., 2014; Melaku Canu et al., 2015; Nerentorp Mastromonaco et al., 2017; Rosati et al., 2018; Zhang et al., 2020), and simulated variations of DMHg (Eq. 4) depend on photodegradation, production upon MMHg methylation and advective transport. MMHg is uptaken from the water pool by phytoplankton ($MMHg_{phy}$) (Sect. 2.3), and it is released from the biotic pool back to the water column by zooplankton excretion ($Ex_{zoo}\frac{MMHg_{zoo}}{C_{zoo}}$) and death ($D_{zoo}\frac{zooMMHg}{C_{zoo}}$) (Sect. 2.4). Loadings, initial and boundary conditions are presented in Sect. 2.6.

2.3 MMHg uptake by phytoplankton in the Hg model

The bioaccumulation model simulates the MMHg uptake by the phytoplankton PFTs of the BFM model assuming that the uptake flux (Eq. (10), $nmol_{(Hg)}\ m^{-3}{}_{(w)}\ d^{-1}$) decreases at high DOC concentrations, and increases proportionally to the phytoplankton Surface Area:Volume ratios, R_{SV_PFT} (Schartup et al., 2018; Zhang et al., 2020). Furthermore, it considers the phytoplankton density (ρ =10^{-12} $g_{(w.w.)}$ $\mu m^{-3}{}_{(w.w.)}$), wet weight biomass ($B_{w.w.,\ PFT}$, in $g_{(w.w.)}\ m^{-3}{}_{(w)}$), and the water MMHg concentrations ($\{MMHg\}_w$, pM). Parameters values are given in Tab. S3.

$$\frac{d\ MMHg_{phy,\ PFT}}{dt} = 0.118 \cdot R_{SV\_PFT} \cdot exp^{(-0.08 \cdot DOC)} \frac{1}{\rho} B_{w.w.,\ PFT} \frac{\{MMHg\}_w}{10^3} \quad (10)$$

$B_{w.w.,\ PFT}$ were derived from the plankton biomasses expressed on a intracellular carbon content basis (C_{PFT}, in $mg_{(C)}/m^3{}_{(w)}$), by adopting a carbon to Wet Weight conversion factors (Tab. S4) that we estimated from a dataset of experimental data for various phytoplankton and zooplankton species (Jørgensen et al., 1979; Mahlmann et al., 2008).

2.4 Zooplankton bioaccumulation in the Hg model

According to previous studies (Schartup et al., 2018; Zhang et al., 2020) MMHg bioaccumulation in zooplankton is mostly driven by grazing (>80%), therefore the trophic transfer of MMHg from phytoplankton to zooplankton PFTs (eterotrophic nanoflagellates, microzooplankton, omnivorous mesozooplankton, and carnivorous mesozooplankton) in the model is set proportionally to the carbon (C) transfer, neglecting direct uptake from seawater. Thus, the bioaccumulation of MMHg in each zooplankton PFT (Eq. (11)) depends on carbon grazing fluxes ($G_{zoo,\ PFT}$, $mg_{(C)}\ m^{-3}\ d^{-1}$) and on the MMHg:C ratio of the preys that are grazed ($\frac{MMHg_{phy,\ PFT}}{C_{phy\ ,\ PFT}}$, $nmol_{(Hg)}/mg_{(C)}$). MMHg release to the water pool occurs following carbon excretion ($Ex_{zoo,\ PFT}$) and zooplankton death ($D_{zoo,\ PFT}$, $mg_{(C)}\ m^{-3}$), and depends on the variable MMHg:C quota ($\frac{MMHg_{zoo,\ PFT}}{C_{zoo,\ PFT}}$, $nmol_{(Hg)}/mg_{(C)}$) in each zooplankton group.

$$\frac{d\ MMHg_{zoo,\ PFT}}{dt} = G_{zoo,\ PFT}\frac{MMHg_{phy,\ PFT}}{C_{phy,\ PFT}} - Ex_{zoo,\ PFT}\frac{MMHg_{zoo,\ PFT}}{C_{zoo,\ PFT}} - D_{zoo,\ PFT}\frac{MMHg_{zoo,\ PFT}}{C_{zoo,\ PFT}} \quad (11)$$

https://doi.org/10.5194/bg-2022-14
Preprint. Discussion started: 14 February 2022

2.5 Indicators for MMHg bioaccumulation and biomagnification

To compare the model content of MMHg in phytoplankton and zooplankton against experimental data, the output in $nmol_{(hg)}/m^3_{(w)}$ were converted into ng $g_{w.w}^{-1}$ by computing the quota of MMHg ($Q_{MMHg,\ PFT}$, Eq. (12)) to plankton wet weight ($B_{w.w.,\ PFT}$, $g_{w.w.}/m^3_{(w)}$) and correcting for the molar mass of Hg (200.59 g/mol).

$$Q_{MMHg,\ PFT} = \frac{MMHg_{phy,\ PFT}}{B_{w.w.,\ PFT}}\ 200.59 \tag{12}$$

The bioconcentration factor (BCF, l/kg) is used to synthesize the enrichment of Hg in plankton with respect to water concentrations (Harding et al., 2018; McGeer et al., 2003), and due to the normalization for MMHg water levels, it allows better intercomparability across ecosystems than Hg concentrations. We calculated BCFs (Eq. (13)) for each plankton PFT as the ratio between the quota $Q_{MMHg,\ PFT}$ and water MMHg concentrations, using model output at monthly resolution spatially averaged. Logarithmic scale is often used to handle BCF values (e.g. McGeer et al., 2003), and thus here the logarithm is included in Eq. (13).

$$\mathrm{BCF} = \log\left(10^6 \frac{\mathrm{Q_{MMHg,\ PFT}}}{\mathrm{MMHg^w}\ 200.59}\right) \tag{13}$$

The trophic magnification factor (TMF) is used to explore biomagnification across ecosystems, by expressing the increase of Hg along trophic levels (Alava et al., 2018; Harding et al., 2018). TMF is usually calculated in field studies of the whole-food web assessing both concentrations of pollutants and trophic levels though nitrogen isotopes. Here, in agreement with other modelling studies (Wu et al., 2021, 2020; Zhang et al., 2020), TMFs were estimated from the ratio of the MMHg quota in zooplankton PFTs to that of grazed phytoplankton PFTs (Eq. (14)). The analysis was carried out considering the model plankton food web as composed by a lower trophic level "herbivorous" part and an upper "omnivorous" part.

$$\mathrm{TMF} = \frac{\mathrm{Q_{MMHg,zoo\text{-}PFTs}}}{\mathrm{Q_{MMHg,\ phy\text{-}PFTs}}} \tag{14}$$

2.6 Initial conditions, boundary conditions and forcings

Initial conditions, boundary conditions and physical forcings for the BFM implementation have monthly resolution, and are set in agreement with Lazzari et al., (2021). Initial conditions (Tab. S5) for Hg species in Mediterranean subbasins (Fig. 3) are extrapolated from published data from different investigations in the Mediterranean Sea (Cossa et al., 2017; Cossa and Coquery, 2005; Ferrara et al., 2003; Horvat et al., 2003; Kotnik et al., 2015, 2007) and boundary conditions are set in agreement with the observations from the GEOTRACES GA03 meridional transect (Bowman et al., 2015). River load is estimated assuming a Hg concentration of 3 pM and 3.5% of MMHg (Cossa et al., 2017). A higher Hg concentration was chosen for three rivers that are known to be highly impacted by mining (Isonzo-Soča river, 25 pM) (Hines et al., 2000), industrial activities (Po river, 6 pM) (Vignati et al., 2008) or both of them (Tiber river, 6 pM) (Lanzillotta et al., 2002;

https://doi.org/10.5194/bg-2022-14
Preprint. Discussion started: 14 February 2022

Rimondi et al., 2019), assuming MMHg was the 1% (Hines et al., 2000). The loading estimate is 6.57 Mg/y, which would be about 70 kg lower (6.49 Mg/y) if we used a uniform Hg concentration of 3 pM. The atmospheric Hg^0 concentrations is set to a constant value Hg^0_{atm}=1.6 ng/m^3 (Andersson et al., 2007; Fantozzi et al., 2013; Gårdfeldt et al., 2003), and the atmospheric deposition of Hg_T is set to 67.5 Mg/y, the 2% of which is MMHg (Cossa et al., 2017). The Hg concentrations in the Black Sea outflow at the Dardanelles strait are set at 0.2 pM in agreement with the observations from the GEOTRACES GA04 cruise and modelled fluxes (Rosati et al., 2018).

2.7 Model sensitivity to POC sinking velocity

The fit against experimental observation has been improved by exploring the importance of the sinking velocity parameter. A sensitivity analysis of POC sinking velocity was carried out, hypothesizing that a change in this parameter would impact the vertical distribution of all Hg species due to a change in the distribution and remineralization of POC, and in the transport of particulate Hg and MeHg. We also speculate that a deeper occurrence of POC remineralization leading to deeper MeHg maximum, could result in a decreased amount of MeHg photochemically degraded and thus in higher MeHg concentrations. In the field, organic particles and aggregates that originate from a continuous size-spectrum of planktonic cells of various composition, show a wide range of sinking speeds (Cael et al., 2021). The current version of BFM model includes only one class of non-living organic detritus (POC) that is a sink for all the plankton state variables (Vichi et al., 2015), resulting in a homogenous POC sinking velocity representative of an ecosystem-averaged dynamic. The base model simulation was run by adopting the default POC sinking velocity of 3 m/d used in previous other works (Lazzari et al., 2021, 2012) to model the biogeochemistry of the Mediterranean Sea. Two additional sensitivity simulations were run, by setting the POC sinking velocity to 10 and 20 m/d, assuming community-averaged cell diameters of 35 and 50 µm, respectively.

2.8 Model sensitivity to the parameterization of Hg methylation

Hg methylation is parameterized in the model by scaling the flux of POC remineralization for a constant x_{met} (Tab. S2), adopting the same value used in a global ocean model (Zhang et al., 2020), due to unavailability of more specific data. We explored the sensitivity of modelled MeHg concentrations to a threefold increase of x_{met}, as well as to an alternative parameterization that included both POC and DOC remineralization flux (Eq. S10).

3 Results and discussion

3.1 MeHg distribution in the water of Mediterranean Sea

The zonal and vertical gradients of MeHg concentrations reproduced by the OGSTM-BFM-Hg model show the highest concentrations in subsurface waters of the most productive subbasins of the Mediterranean Sea (Fig. 4), consistently with the available observations (Cossa et al., 2009). Modelled vertical profiles of MeHg concentrations (Fig. 5) are in good agreement

https://doi.org/10.5194/bg-2022-14
Preprint. Discussion started: 14 February 2022

with the observations in the Southern Adriatic Sea (SAD, Fig. 5a), and are in the lower range of the observations for the North Western Mediterranean (NWM, Fig. 5b) and Ionian (ION, Fig. 5c) subbasins.

The sensitivity analysis showed that the sinking speed is an important control on the vertical distribution of MeHg (i.e., the shape of the vertical profile) in the water column but has little effect on the values of concentrations maxima (Supplemental Sect. S1 and Fig. S1). The sensitivity also showed that MeHg concentrations increase at depths where concentrations maxima have been observed (Cossa et al., 2009) if a threefold increase in the coefficient x_{met} is assumed (Supplemental Sect. S1 and Fig. S2), while the inclusion of DOC remineralization flux result in an excessive increase of surficial MeHg concentrations. Modelled concentrations of Hg_T (Fig. S3) are within the experimental uncertainty of the data used to initialize the model, thus Hg methylation in the model does not appear to be limited by availability of inorganic Hg, and a calibration of the parameter x_{met} appears appropriate, considering that the initial guess for this parameter came from a global ocean application (Zhang et al., 2020). Indeed, such a global model study underestimated the observed MeHg concentrations in the Mediterranean Sea, while reproducing with good agreement, or overestimating, observations from various cruises in the North Atlantic and Pacific Ocean, pointing out the need to better resolve spatial and temporal variability of biological processes and linked Hg dynamics (Zhang et al., 2020). In spite of uncertainties remaining to be addressed, the OGSTM-BFM-Hg model is able to reproduce observed spatial gradients, testifying the improvements in capability to simulate Hg dynamics (Žagar et al., 2014, 2007) through the coupling with key biological processes, e.g. the carbon pump and microbial loop (Bowman et al., 2020; Cossa et al., 2017, 2009; Heimbürger et al., 2010; Monperrus et al., 2007; Munson et al., 2018; Sunderland et al., 2009).

Seasonality affects the modelled distribution of MeHg (Fig. 4 and 5) with more marked effects in the SAD subbasin (Fig. 5a). The strong winter convection occurring in the SAD in 2017 caused remixing in the water column (Mihanović et al., 2021) leading to the disruption of the subsurface MeHg maximum from January to March and to an increase in MeHg surface water concentrations, in spite of net demethylation prevailing at all depths during winter months (Fig. 6). A slighter increase in surface water MeHg concentrations during winter months is visible also for the other subbasins (Fig. 4, 5b and 5c) but, in the absence of strong winter convection the variation is small, and the model predicts that the subsurface MeHg maximum is a permanent feature throughout the year. The NWM is known to be an area of winter convection, however other authors reported a recent decline of deep convection for this area that was weak in 2014 and never occurred in the period 2015-2017 (Margirier et al., 2020). Based on these model results, we speculate that in the long run the reduction of winter mixing can cause MeHg accumulation in the biological active zone enhancing marine organisms exposure.

In the SAD subbasin, a progressive buildup of MeHg subsurface maxima (up to 0.18 pM) is predicted from April to September, driven by an increase in primary production triggering higher POC remineralization and in turn higher Hg methylation rate constants kmet (Fig. S4). However, while kmet are maxima in April, and net methylation fluxes (Fig. 6) are maxima in June (0.45 pmol m^{-3} d^{-1}), MeHg concentrations are maxima in September and remain stable until October (Fig. 5), highlighting the importance of water stratification for the formation of the subsurface maxima. Figure 6 also shows that net MeHg demethylation prevails throughout the year in deep waters (with the exception of a weak positive methylation in SAD and

https://doi.org/10.5194/bg-2022-14
Preprint. Discussion started: 14 February 2022

TYR during summer), and for most of the year in surface waters. This suggests that the presence of MeHg in surface and deep water depends on its formation in the intermediate waters and diapycnal mixing.

Modelled vertical profiles of MeHg in the oligotrophic ION subbasin (Fig. 5c) have lower maxima (up to 0.16 pM) and a smoother concentration gradient compared to the more productive waters of the NWM (up to 0.24 pM). The West-East gradient is sustained by the highest methylation rates (Fig. S4) in the Western Mediterranean, driven by higher primary productivity and remineralization of organic detritus, and it is further reinforced by high rates of both photochemical and biological MeHg degradation in the Eastern subbasins (Fig. S4), due to the highest water temperature, irradiance, and deeper penetration of shortwave radiation due to the low plankton biomass.

3.2 Modelled MMHg in phytoplankton and zooplankton

The spatial and temporal distributions (Fig. 7) of modelled MMHg in phytoplankton ($MMHg_{phy}$) and zooplankton ($MMHg_{zoo}$) of the Mediterranean Sea are overall comparable to the concentrations of particulate MMHg (0.7 ± 1.3 pmol m^{-3}) measured in the Atlantic Ocean (Bowman et al., 2015). The model reproduced a seasonal increase in $MMHg_{phy}$ (Fig. 7a) during late spring and summer that is driven by blooms of picophytoplankton (Fig. S5) combined with an increase in MMHg availability in surface water (Fig. S6). The amount of MMHg bioaccumulated by picophytoplankton ($MMHg_{phy,P3}$, Fig. S7) is high (up to 0.6 $pmol_{(hg)}\ m_{(w)}^{-3}$) compared to the bioaccumulation by other phytoplankton PFTs (up to 0.02 $pmol_{(hg)}\ m_{(w)}^{-3}$, Fig. S8-S10) due to the model assumption of increasing bioconcentration capacity with decreasing phytoplankton cell size (Sect. 2.3). However, not all the picophytoplankton blooms results in high values of $MMHg_{phy}$: the strongest blooms of picophytoplankton, occurring in March and April at 25 m depth (Fig. S5), have a marginal impact on bioaccumulation, especially in the easternmost subbasins, due to the very low concentrations of MMHg in the most surficial waters (Fig. S6). On the other hand, much weaker blooms of picophytoplankton occurring from May to August slightly deeper in the water column (35 and 45 m depth) lead to a maximum in phytoplankton MMHg concentrations (Fig. 7a) because of higher water MMHg concentrations at these depths during these months (Fig. S6). The average $MMHg_{phy,P3}$ is lower in the ALB subbasin than in the SAD subbasin (Tab. 1), the latter being characterized by higher availability of MMHg at 35-45 m depth and higher biomassess of picophytoplankton during summer (Fig. S5 and S6). The hypothesis of the cell size-effect on bioconcentration is the best synthesis of available knowledge (Schartup et al., 2018), however the experimental study from which this relationship was derived, also showed deviations from this pattern and temperature induced effects, possibly due to phagocytosis of Hg-OM compounds by mixotroph organisms such as dynoflagellates (Lee and Fisher, 2016). One of the few field studies assessing the size-effect on Hg bioaccumulation in plankton (Gosnell and Mason, 2015) found an increase in MeHg% but not in MeHg content for smaller plankton size (< 5 µm), however the size classes analysed by that study do not overlap well with the functional groups of OGSTM-BFM-Hg model. More field, in vitro and modelling studies are needed to disentangle the dynamics underlying key processes for Hg bioaccumulation.

The highest concentrations of $MMHg_{zoo}$ (Fig. 7b) are predicted from June to September at 35 m-depth, showing a delay of about one month with respect to the temporal evolution of $MMHg_{phy}$ due to the combined impacts of plankton phenology and

https://doi.org/10.5194/bg-2022-14
Preprint. Discussion started: 14 February 2022

trophic interactions. Heterotrophic nanoflagellates bioaccumulate much more MMHg (up to 0.5 pmol/m3, Fig. S11) than other zooplankton PFTs (up to 0.1 pmol m-3, Fig. S12-S14) because they feed on picophytoplankton (Fig. 8) which is more enriched in MeHg than other PFTs, and are an important driver for the distribution of $MMHg_{zoo}$. However, in spite of heterotrophic nanoflagellates being always abundant from March to October (Fig. S15), and most abundant in the eastern subbasins, the highest MMHg bioaccumulation occurs when the increase of the nanoflagellates population is coincident with an enrichment of MMHg in phytoplankton (i.e., in western subbasins, as well as in the Adriatic and part of the Ionian Sea during summer).

The mean MMHg quota ($Q_{MMHg,PFT}$) in phytoplankton of the Mediterranean Sea is about 3.0 ng $g_{w.w}^{-1}$ for picophytoplankton, 0.3 ng $g_{w.w}^{-1}$ for autotrophic nanoflagellates, 0.03 ng $g_{w.w}^{-1}$ for diatoms, and 0.04 ng $g_{w.w}^{-1}$ for large phytoplankton. The spatial variability is highlighted by the comparison of the quotas estimated for the ALB and SAD subbasins (Tab. 1) that are in the lower and upper range of the vales for the Mediterranean Sea. Modelled values are comparable with the few observations available for open waters of the central Pacific Ocean (0.1-4 ng $g_{w.w}^{-1}$) (Gosnell & Mason, 2015), and of the Northwest Atlantic Ocean (0.15 ± 0.06 ng $g_{w.w}^{-1}$) (Hammerschmidt et al., 2013), as well as with data from various coastal and shelf ecosystems (Harding et al., 2018). The speciation of Hg in phytoplankton groups of the Mediterranean Sea has never been assessed (Cinnirella et al., 2019). The MMHg quota was about 0.14 ± 0.1 ng $g_{w.w}^{-1}$ in seston of diameter 80–200 µm sampled in the Gulf of Lions during spring and autumn 2004-2006 (Cossa et al., 2012).

The mean $Q_{MMHg,PFT}$ in zooplankton are 0.8 ng $g_{w.w}^{-1}$ for heterotrophic nanoflagellates, 0.3 ng $g_{w.w}^{-1}$ for microzooplankton, 0.6 ng $g_{w.w}^{-1}$ for omnivorous mesozooplankton, and 0.9 ng $g_{w.w}^{-1}$ for carnivorous mesozooplankton. The MMHg quota in carnivorous zooplankton ($Q_{MMHg,Z3}$) estimated for the SAD subbasin is much higher (3.60 ±2.2) than the average value, due to the high MMHg accumulation in the whole food web (Tab. 1). However, since biomasses of carnivorous zooplankton in the SAD are very low (Fig. S16), the overall content of MMHg in this group ($MMHg_{zoo,Z3}$) is lower ($1.0\ 10^{-3} \pm 2.7\ 10^{-4}$) than in the ALB subbasin ($1.9\ 10^{-2} \pm 1.6\ 10^{-3}$).

The modelled zooplankton quotas compares well with the observations of MMHg in mesozooplankton of the Gulf of Lions, which was 0.52 ± 0.39 ng $g_{w.w}^{-1}$ for the size range 200-500 µm, 0.57± 0.39 ng $g_{w.w}^{-1}$ for the size range 500-1000 µm, and 1.8 ± 1.3 ng $g_{w.w}^{-1}$ for zooplankton >200 µm (Cossa, 2012). MMHg measured in the '90s in zooplankton in the Hg hotspot of Gulf of Trieste (NAD, Fig. 3) was 2.1 ± 2.3 ng $g_{w.w}^{-1}$ (Horvat et al., 2014, 1999), consistently with the fact that the Gulf of Trieste is an upper bound for the Mediterranean, being subjected to high loadings of legacy Hg from the Soca-Isonzo river (Hines et al., 2000) and coastal lagoons (Melaku Canu et al., 2015).

3.3 Bioconcentration Factors and Trophic Magnification Factors

Modelled BCFs for phytoplankton PFTs of the Mediterranean Sea range 3.7-6.5, which is slightly lower than the range (4.3-6.8) reported for phytoplankton from the central Pacific (Gosnell and Mason, 2015) and is higher than the ranges for Long Island Sound (2.6-5.5) (Gosnell et al., 2017) and other coastal and shelf sites of the world (3.1-4.4) (Harding et al., 2018). Higher BCFs in open waters than in coastal areas are consistent with the enhanced Hg bioavailability in the open sea inferred by other authors (Gosnell and Mason, 2015; Schartup et al., 2015), which in the model is approximated through the inverse

https://doi.org/10.5194/bg-2022-14
Preprint. Discussion started: 14 February 2022

relationship between MMHg uptake and DOC (Eq. (10)). Modelled zooplankton BCFs in the Mediterranean Sea span from 4.0 to 6.4, comparable to the BCFs estimated for mesozooplankton (4.0-6.5) in the Pacific Ocean (Gosnell and Mason, 2015). The trophic interactions among PFTs simulated by the model can be subdivided into a lower "herbivorous" part of the food web and an upper "omnivorous" part of the food web (Fig. 8). In the lower part of the food web, heterotrophic nanoflagellates (2-20 μm) grazes on bacteria (<1 μm) and picophytoplankton (0.2-2 μm), while microzooplankton (20 – 200 μm) grazes on heterotrophic and autotrophic nanoflagellates (2-20 μm), diatoms (200- 20 μm), and occasionally on other PFTs. In the upper part of the food web, the omnivorous mesozooplankton (200-2000 μm) preys on microzooplankton and on all the phytoplankton PFTs>2 μm, while carnivorous mesozooplankton (200-2000 μm) preys on omnivorous mesozooplankton and large phytoplankton (>100 μm). The highest BCFs (and $Q_{MMHg,PFT}$) are predicted for picophytoplankton and carnivorous zooplankton (Tab. 1 and Fig. 8). Heterotrophic nanoflagellates display lower bioaccumulation than picophytoplankton because they also feed on bacteria and autotrophic nanoflagellates that 'dilute' the MMHg intake (Fig. 8). Microzooplankton and omnivorous zooplankton, which have an intermediate position in the food web, have bioaccumulation levels comparable to those of heterotrophic nanoflagellates. The effect of biomagnification is visible only in carnivorous zooplankton, having much higher BCFs than their prey (Tab. 1). These dynamics are consistent with a global model taking into account a more complex plankton food web (366 PFTs) that found highest MMHg levels in phytoplankton than in their predators, and biomagnification in the highest trophic levels with high food intake (Wu et al., 2021).

Trophic magnification factors (TMFs) were calculated for each subbasin of the Mediterreanean Sea for the lower and upper parts of the food web. Low TMFs (range 0.05-0.38) were estimated for the lower food web indicating absence of biomagnification (Fig. 9a), and higher TMFs (range 0.15-2.60) were estimated for the upper food web (Fig. 9b), in agreement with previous modelling studies suggesting that MMHg biomagnification between small zooplankton groups and phytoplankton is unlikely to happen (Wu et al., 2021, 2020; Zhang et al., 2020). Biomagnification (TMF>1) in the upper food web (Fig. 9b) occurs only in Mediterranean subbasins with relatively abundant biomasses of carnivorous zooplankton (Fig. S16), namely in the ALB and SWM subbasins. The TMF for the ALB subbasin (2.4±0.28) is lower than but comparable to the biomagnification from microseston to zooplankton (TMF=4) estimated from field data for the Northwest Atlantic Ocean (Hammerschmidt et al., 2013). The other Mediterranean subbasins, due to the absence or very low abundance of carnivorous mesozooplankton (<0.05 $mg_{(C)}$ m^{-3}), have a shorter food web and lower TMFs (<1). Although oligotrophy tends to favour longer food webs enhancing biomagnification, in extremely oligotrophic ecosystems the very low primary production can limit the presence of carnivorous zooplankton populations, lowering the bioaccumulation potential (Wu et al., 2021). The TMFs<1 for the upper part of the food web are comparable to the estimates made with a global model for the most oligotrophic ocean regions such as the South Pacific gyre, the North Atlantic gyre, and the South Atlantic gyre (Wu et al., 2021).

https://doi.org/10.5194/bg-2022-14
Preprint. Discussion started: 14 February 2022

4 Conclusions

We developed the OGSTM-BFM-Hg model, a numerical state of the art model tracking the biogeochemistry of the main marine Hg species (Hg^{II}, Hg^0, MMHg, and DMHg) coupled to the biogeochemistry of plankton and nutrients. The model, applied to a high resolution 3D domain of the Mediterranean Sea, successfully captured the zonal and vertical variability of MeHg concentrations reproducing a decreasing MeHg gradient from West to East that is supported by the available observations. Sensitivity analysis showed that the agreement with observations of MeHg was improved by adopting an intermediate sinking speed for organic detritus and by increasing the rate constant for Hg methylation, while the inclusion in the equation for methylation of the remineralization of dissolved carbon (DOC) increases the mismatch between model and observations, suggesting that this process might not be important in shaping MeHg distributions.

Model results highlight that summer stratification of the water column is an important process for the buildup of a sub-surficial maximum of MeHg concentrations, while the occurrence of deep convection in winter result in substantial redistribution of MeHg smoothing the vertical profiles. A decrease of winter convection events linked to increasing water temperature, which has already been observed in recent years in the Mediterranean Sea, seems to limit MeHg redistribution in the water column causing higher waters MeHg concentrations in the biologically active zone and, in turn, higher plankton exposure. In fact, spatial and temporal variability of plankton bioaccumulation in the model is controlled by plankton phenology and by the availability of MMHg at the depths at which plankton blooms occur. The biomagnification potential is stronger in productive areas of the Mediterranean Sea characterized by high biodiversity and longer food web length with a significant presence of carnivorous zooplankton, such as the ALB and SWM subbasins.

Acknowledgments

The research has been partially funded by the PRIN project ICCC (Impacts of climate change on the biogeochemistry of contaminants in the Mediterranean Sea).

Code availability

The OGSTM-BFM-Hg model code is publicly available at Zenodo repository with DOI https://doi.org/10.5281/zenodo.5851442 (Rosati et al., 2022).

References

Alava, J. J., Cisneros-Montemayor, A. M., Sumaila, U. R. and Cheung, W. W. L.: Projected amplification of food web bioaccumulation of MeHg and PCBs under climate change in the Northeastern Pacific, Sci. Rep., 8(1), 1–12, doi:10.1038/s41598-018-31824-5, 2018.

https://doi.org/10.5194/bg-2022-14
Preprint. Discussion started: 14 February 2022

Amos, H. M., Sonke, J. E., Obrist, D., Robins, N., Hagan, N., Horowitz, H. M., Mason, R. P., Witt, M., Hedgecock, I. M., Corbitt, E. S. and Sunderland, E. M.: Observational and modelling constraints on global anthropogenic enrichment of mercury, Environ. Sci. Technol., 49(7), 4036–4047, doi:10.1021/es5058665, 2015.

An, J., Zhang, L., Lu, X., Pelletier, D. A., Pierce, E. M., Johs, A., Parks, J. M. and Gu, B.: Mercury Uptake by Desulfovibrio desulfuricans ND132: Passive or Active?, Environ. Sci. Technol., 53(11), 6264–6272, doi:10.1021/acs.est.9b00047, 2019.

Andersson, M. E., Gårdfeldt, K., Wängberg, I., Sprovieri, F., Pirrone, N. and Lindqvist, O.: Reprint of "Seasonal and daily variation of mercury evasion at coastal and off shore sites from the Mediterranean Sea," Mar. Chem., 107(1), 104–116, doi:10.1016/j.marchem.2007.06.020, 2007.

Baya, P. A., Gosselin, M., Lehnherr, I., St. Louis, V. L. and Hintelmann, H.: Determination of monomethylmercury and dimethylmercury in the arctic marine boundary layer, Environ. Sci. Technol., doi:10.1021/es502601z, 2015.

Blum, J. D., Popp, B. N., Drazen, J. C., Anela Choy, C. and Johnson, M. W.: Methylmercury production below the mixed layer in the North Pacific Ocean, Nat. Geosci., 6(10), 879–884, doi:10.1038/ngeo1918, 2013.

Bowman, K. L., Hammerschmidt, C. R., Lamborg, C. H. and Swarr, G.: Mercury in the North Atlantic Ocean: The U.S. GEOTRACES zonal and meridional sections, Deep. Res. Part II Top. Stud. Oceanogr., 116, 251–261, doi:10.1016/j.dsr2.2014.07.004, 2015.

Bowman, K. L., Hammerschmidt, C. R., Lamborg, C. H., Swarr, G. J. and Agather, A. M.: Distribution of mercury species across a zonal section of the eastern tropical South Pacific Ocean (U.S. GEOTRACES GP16), Mar. Chem., 186, 156–166, doi:10.1016/j.marchem.2016.09.005, 2016.

Bowman, K. L., Lamborg, C. H. and Agather, A. M.: A global perspective on mercury cycling in the ocean, Sci. Total Environ., 710, 136166, doi:10.1016/j.scitotenv.2019.136166, 2020.

Cael, B. B., Cavan, E. L. and Britten, G. L.: Reconciling the Size-Dependence of Marine Particle Sinking Speed, Geophys. Res. Lett., 48(5), 1–11, doi:10.1029/2020GL091771, 2021.

Canu, D. and Rosati, G.: Long-term scenarios of mercury budgeting and exports for a Mediterranean hot spot (Marano-Grado Lagoon, Adriatic Sea)., Estuar. Coast. Shelf Sci., 198, 518–528, doi:10.1016/j.ecss.2016.12.005, 2017.

Canu, D., Ghermandi, A., Nunes, P. A. L. D., Lazzari, P., Cossarini, G. and Solidoro, C.: Estimating the value of carbon sequestration ecosystem services in the mediterranean sea: An ecological economics approach, Glob. Environ. Chang., 32, 87–95, doi:10.1016/j.gloenvcha.2015.02.008, 2015.

Canu, D. M., Rosati, G. and Solidoro, C.: Mercury Budget and Scenario Analysis for the Marano-Grado Lagoon, Using Modelling and Observations, Proc., 30(1), doi:10.3390/proceedings2019030019, 2019.

Choe, K.-Y. and Gill, G. a.: Distribution of particulate, colloidal, and dissolved mercury in San Francisco Bay estuary. 2. Monomethyl mercury, Limnol. Oceanogr., 48(4), 1547–1556, doi:10.4319/lo.2003.48.4.1547, 2003.

Choe, K.-Y., Gill, G. A. and Lehman, R.: Distribution of particulate, colloidal, and dissolved mercury in San Francisco Bay estuary. 1. Total mercury, Limnol. Oceanogr., 48(4), 1535–1546, doi:10.4319/lo.2003.48.4.1547, 2003.

Cinnirella, S., Bruno, D. E., Pirrone, N., Horvat, M., Živković, I., Evers, D. C., Johnson, S. and Sunderland, E. M.: Mercury concentrations in biota in the Mediterranean Sea, a compilation of 40 years of surveys, Sci. data, 6(1), 205, doi:10.1038/s41597-019-0219-y, 2019.

Coale, K. H., Heim, W. A., Negrey, J., Weiss-Penzias, P., Fernandez, D., Olson, A., Chiswell, H., Byington, A., Bonnema, A., Martenuk, S., Newman, A., Beebe, C. and Till, C.: The distribution and speciation of mercury in the California current: Implications for mercury transport via fog to land, Deep. Res. Part II Top. Stud. Oceanogr., 151(May), 77–88, doi:10.1016/j.dsr2.2018.05.012, 2018.

Conaway, C. H., Black, F. J., Gault-Ringold, M., Pennington, J. T., Chavez, F. P. and Flegal, A. R.: Dimethylmercury in coastal upwelling waters, Monterey Bay, California, Environ. Sci. Technol., 43(5), 1305–1309, doi:10.1021/es802705t, 2009.

Cossa, D.: Supporting Information (19 pages), , (L), 1–19, 2012.

Cossa, D. and Coquery, M.: The Mediterranean Mercury Anomaly, a Geochemical or a Biologocal Issue, in The Mediterranean Sea, edited by A. Saliot, pp. 177–208, Springer Berlin Heidelberg, Berlin, Heidelberg., 2005.

Cossa, D., Averty, B. and Pirrone, N.: The origin of methylmercury in open Mediterranean waters, Limnol. Oceanogr., 54(3), 837–844, doi:10.4319/lo.2009.54.3.0837, 2009.

Cossa, D., Harmelin-Vivien, M., Mellon-Duval, C., Loizeau, V., Averty, B., Crochet, S., Chou, L. and Cadiou, J.-F.: Influences of bioavailability, trophic position, and growth on methylmercury in hakes (Merluccius merluccius) from Northwestern Mediterranean and Northeastern Atlantic., Environ. Sci. Technol., 46(9), 4885–93, doi:10.1021/es204269w, 2012.

Cossa, D., Durrieu de Madron, X., Schäfer, J., Lanceleur, L., Guédron, S., Buscail, R., Thomas, B., Castelle, S. and Naudin, J.-J.: The open sea as the main source of methylmercury in the water column of the Gulf of Lions (Northwestern Mediterranean margin), Geochim. Cosmochim. Acta, 199, 222–237, doi:10.1016/j.gca.2016.11.037, 2017.

Cossarini, G., Lazzari, P. and Solidoro, C.: Spatiotemporal variability of alkalinity in the Mediterranean Sea, Biogeosciences, 12(6), 1647–1658, doi:10.5194/bg-12-1647-2015, 2015.

Cossarini, G., Feudale, L., Teruzzi, A., Bolzon, G., Coidessa, G., Solidoro, C., Di Biagio, V., Amadio, C., Lazzari, P., Brosich, A. and Salon, S.: High-Resolution Reanalysis of the Mediterranean Sea Biogeochemistry (1999–2019), Front. Mar. Sci., 8(November), 1–21, doi:10.3389/fmars.2021.741486, 2021.

Fantozzi, L., Manca, G., Ammoscato, I., Pirrone, N. and Sprovieri, F.: The cycling and sea-air exchange of mercury in the waters of the Eastern Mediterranean during the 2010 MED-OCEANOR cruise campaign, Sci. Total Environ., 448, 151–162, doi:10.1016/j.scitotenv.2012.09.062, 2013.

Ferrara, R., Ceccarini, C., Lanzillotta, E., Gårdfeldt, K., Sommar, J., Horvat, M., Logar, M., Fajon, V. and Kotnik, J.: Profiles of dissolved gaseous mercury concentration in the Mediterranean seawater, Atmos. Environ., 37(SUPPL. 1), 85–92, doi:10.1016/S1352-2310(03)00248-6, 2003.

Gårdfeldt, K., Sommar, J., Ferrara, R., Ceccarini, C., Lanzillotta, E., Munthe, J., Wängberg, I., Lindqvist, O., Pirrone, N., Sprovieri, F., Pesenti, E. and Strömberg, D.: Evasion of mercury from coastal and open waters of the Atlantic Ocean and the Mediterranean Sea, Atmos. Environ., 37, 73–84, doi:10.1016/S1352-2310(03)00238-3, 2003.

https://doi.org/10.5194/bg-2022-14
Preprint. Discussion started: 14 February 2022

Gosnell, K. J. and Mason, R. P.: Mercury and methylmercury incidence and bioaccumulation in plankton from the central Pacific Ocean, Mar. Chem., 177, 772–780, doi:10.1016/j.marchem.2015.07.005, 2015.

Gosnell, K. J., Balcom, P. H., Tobias, C. R., Gilhooly, W. P. and Mason, R. P.: Spatial and temporal trophic transfer dynamics of mercury and methylmercury into zooplankton and phytoplankton of Long Island Sound, Limnol. Oceanogr., 62(3), 1122–1138, doi:10.1002/lno.10490, 2017.

Hammerschmidt, C. R., Finiguerra, M. B., Weller, R. L. and Fitzgerald, W. F.: Methylmercury Accumulation in Plankton on the Continental Margin of the Northwest Atlantic Ocean, Environ. Sci. Technol., 47, 3671–3677, 2013.

Harding, G., Dalziel, J. and Vass, P.: Bioaccumulation of methylmercury within the marine food web of the outer Bay of Fundy, Gulf of Maine, PLoS One, 13(7), 1–30, doi:10.1371/journal.pone.0197220, 2018.

Harmelin-Vivien, M., Cossa, D., Crochet, S., Bănaru, D., Letourneur, Y. and Mellon-Duval, C.: Difference of mercury bioaccumulation in red mullets from the north-western Mediterranean and Black seas, Mar. Pollut. Bull., 58(5), 679–685, doi:10.1016/j.marpolbul.2009.01.004, 2009.

Heimbürger, L.-E., Cossa, D., Marty, J.-C., Migon, C., Averty, B., Dufour, A. and Ras, J.: Methylmercury distributions in relation to the presence of nano- and picophytoplankton in an oceanic water column (Ligurian Sea, North-western Mediterranean), Geochim. Cosmochim. Acta, 74(19), 5549–5559, doi:10.1016/j.gca.2010.06.036, 2010.

Hines, M. E., Horvat, M., Faganeli, J., Bonzongo, J. C. J., Barkay, T., Major, E. B., Scott, K. J., Bailey, E. A., Warwick, J. J. and Lyons, W. B.: Mercury biogeochemistry in the Idrija River, Slovenia, from above the mine into the Gulf of Trieste, Environ. Res., 83(2), 129–139, doi:10.1006/enrs.2000.4052, 2000.

Horvat, M., Covelli, S., Faganeli, J., Logar, M., Mandić, V., Rajar, R., Širca, A. and Žagar, D.: Mercury in contaminated coastal environments; a case study: The Gulf of Trieste, Sci. Total Environ., 237–238, 43–56, doi:10.1016/S0048-9697(99)00123-0, 1999.

Horvat, M., Kotnik, J., Logar, M., Fajon, V., Zvonarić, T. and Pirrone, N.: Speciation of mercury in surface and deep-sea waters in the Mediterranean Sea, Atmos. Environ., 37, Supple(0), 93–108, doi:http://dx.doi.org/10.1016/S1352-2310(03)00249-8, 2003.

Horvat, M., Degenek, N., Lipej, L., Snoj Tratnik, J. and Faganeli, J.: Trophic transfer and accumulation of mercury in ray species in coastal waters affected by historic mercury mining (Gulf of Trieste, northern Adriatic Sea), Environ. Sci. Pollut. Res., 21(6), 4163–4176, doi:10.1007/s11356-013-2262-0, 2014.

Jonsson, S., Mazrui, N. M. and Mason, R. P.: Dimethylmercury Formation Mediated by Inorganic and Organic Reduced Sulfur Surfaces, Sci. Rep., 6(August), 27958, doi:10.1038/srep27958, 2016.

Jørgensen, S. E., Friis, M. B., Henriksen, J., Jørgensen, L. A. and Mejer, H. F.: Handbook of Envirnmental Data and Ecological Parameters, edited by S. E. Jørgensen, Pergamon Press, International Society for Ecological Modelling., 1979.

Kotnik, J., Horvat, M., Tessier, E., Ogrinc, N., Monperrus, M., Amouroux, D., Fajon, V., Gibičar, D., Žižek, S., Sprovieri, F. and Pirrone, N.: Mercury speciation in surface and deep waters of the Mediterranean Sea, Mar. Chem., 107(1), 13–30, doi:10.1016/j.marchem.2007.02.012, 2007.

Kotnik, J., Horvat, M., Ogrinc, N., Fajon, V., Žagar, D., Cossa, D., Sprovieri, F. and Pirrone, N.: Mercury speciation in the Adriatic Sea, Mar. Pollut. Bull., 96(1–2), 136–148, doi:10.1016/j.marpolbul.2015.05.037, 2015.

Lamborg, C. H., Hammerschmidt, C. R., Bowman, K. L., Swarr, G. J., Munson, K. M., Ohnemus, D. C., Lam, P. J., Heimbürger, L.-E., Rijkenberg, M. J. A. and Saito, M. A.: A global ocean inventory of anthropogenic mercury based on water column measurements, Nature, 512(7512), 65–68, doi:10.1038/nature13563, 2014.

Lamborg, C. H., Hammerschmidt, C. R. and Bowman, K. L.: An examination of the role of particles in oceanic mercury cycling, Philos. Trans. R. Soc. A Math. Phys. Eng. Sci., 374(2081), 20150297, doi:10.1098/rsta.2015.0297, 2016.

Lanzillotta, E., Ceccarini, C. and Ferrara, R.: Photo-induced formation of dissolved gaseous mercury in coastal and offshore seawater of the Mediterranean basin, Sci. Total Environ., 300(1–3), 179–187, doi:10.1016/S0048-9697(02)00223-1, 2002.

Lazzari, P., Teruzzi, A., Salon, S., Campagna, S., Calonaci, C., Colella, S., Tonani, M. and Crise, A.: Pre-operational short-term forecasts for Mediterranean Sea biogeochemistry, Ocean Sci., 6(1), 25–39, doi:10.5194/os-6-25-2010, 2010.

Lazzari, P., Solidoro, C., Ibello, V., Salon, S., Teruzzi, A., Béranger, K., Colella, S. and Crise, A.: Seasonal and inter-annual variability of plankton chlorophyll and primary production in the Mediterranean Sea: A modelling approach, Biogeosciences, 9(1), 217–233, doi:10.5194/bg-9-217-2012, 2012.

Lazzari, P., Mattia, G., Solidoro, C., Salon, S., Crise, A., Zavatarelli, M., Oddo, P. and Vichi, M.: The impacts of climate change and environmental management policies on the trophic regimes in the Mediterranean Sea: Scenario analyses, J. Mar. Syst., 135, 137–149, doi:10.1016/j.jmarsys.2013.06.005, 2014.

Lazzari, P., Solidoro, C., Salon, S. and Bolzon, G.: Spatial variability of phosphate and nitrate in the Mediterranean Sea: A modelling approach, Deep. Res. Part I Oceanogr. Res. Pap., 108(January), 39–52, doi:10.1016/j.dsr.2015.12.006, 2016.

Lazzari, P., Álvarez, E., Terzić, E., Cossarini, G., Chernov, I., D'ortenzio, F. and Organelli, E.: Cdom spatiotemporal variability in the mediterranean sea: A modelling study, J. Mar. Sci. Eng., 9(2), 1–18, doi:10.3390/jmse9020176, 2021.

Lee, C. and Fisher, N. S.: Methylmercury uptake by diverse marine phytoplankton, Limnol. Oceanogr., 61, 1626–1639, doi:10.1002/lno.10318, 2016.

Lehnherr, I., St. Louis, V. L., Hintelmann, H. and Kirk, J. L.: Methylation of inorganic mercury in polar marine waters, Nat. Geosci., 4(April), 298–302, doi:10.1038/ngeo1134, 2011.

Luo, H., Cheng, Q. and Pan, X.: Photochemical behaviors of mercury (Hg) species in aquatic systems: A systematic review on reaction process, mechanism, and influencing factor, Sci. Total Environ., 720, 137540, doi:10.1016/j.scitotenv.2020.137540, 2020.

Mahlmann, D. M., Jahnke, J. and Loosen, P.: Rapid determination of the dry weight of single, living cyanobacterial cells using the Mach-Zehnder double-beam interference microscope, Eur. J. Phycol., 43(4), 355–364, doi:10.1080/09670260802168625, 2008.

Margirier, F., Testor, P., Heslop, E., Mallil, K., Bosse, A., Houpert, L., Mortier, L., Bouin, M. N., Coppola, L., D'Ortenzio, F., Durrieu de Madron, X., Mourre, B., Prieur, L., Raimbault, P. and Taillandier, V.: Abrupt warming and salinification of

https://doi.org/10.5194/bg-2022-14
Preprint. Discussion started: 14 February 2022

intermediate waters interplays with decline of deep convection in the Northwestern Mediterranean Sea, Sci. Rep., 10(1), 1–11, doi:10.1038/s41598-020-77859-5, 2020.

Mason, R. P., Choi, A. L., Fitzgerald, W. F., Hammerschmidt, C. R., Lamborg, C. H., Soerensen, A. L. and Sunderland, E. M.: Mercury biogeochemical cycling in the ocean and policy implications, Environ. Res., 119, 101–117, doi:10.1016/j.envres.2012.03.013, 2012.

McGeer, J. C., Brix, K. V., Skeaff, J. M., Deforest, D. K., Brigham, S. I., Adams, W. J. and Green, A.: Inverse relationship between bioconcentration factor and exposure concentration for metals: Implications for hazard assessment of metals in the aquatic environment, Environ. Toxicol. Chem., 22(5), 1017–1037, doi:10.1897/1551-5028(2003)022<1017:IRBBFA>2.0.CO;2, 2003.

Melaku Canu, D., Rosati, G., Solidoro, C., Heimbürger, L.-E. and Acquavita, A.: A comprehensive assessment of the mercury budget in the Marano–Grado Lagoon (Adriatic Sea) using a combined observational modeling approach, Mar. Chem., 177, 742–752, doi:10.1016/j.marchem.2015.10.013, 2015.

Mihanović, H., Vilibić, I., Šepić, J., Matić, F., Ljubešić, Z., Mauri, E., Gerin, R., Notarstefano, G. and Poulain, P. M.: Observation, Preconditioning and Recurrence of Exceptionally High Salinities in the Adriatic Sea, Front. Mar. Sci., 8(July), 1–22, doi:10.3389/fmars.2021.672210, 2021.

Monperrus, M., Tessier, E., Amouroux, D., Leynaert, A., Huonnic, P. and Donard, O. F. X.: Mercury methylation, demethylation and reduction rates in coastal and marine surface waters of the Mediterranean Sea, Mar. Chem., 107(1), 49–63, doi:10.1016/j.marchem.2007.01.018, 2007.

Motta, L. C., Blum, J. D., Johnson, M. W., Umhau, B. P., Popp, B. N., Washburn, S. J., Drazen, J. C., Benitez-Nelson, C. R., Hannides, C. C. S., Close, H. G. and Lamborg, C. H.: Mercury Cycling in the North Pacific Subtropical Gyre as Revealed by Mercury Stable Isotope Ratios, Global Biogeochem. Cycles, 33(6), 777–794, doi:10.1029/2018GB006057, 2019.

Munson, K. M., Lamborg, C., Swarr, G. J. and Saito, M. A.: Mercury species concentrations and fluxes in the Central Tropical Pacific Ocean, Global Biogeochem. Cycles, 29(Ii), 656–676, doi:10.1002/2015GB005120.Received, 2015.

Munson, K. M., Lamborg, C. H., Boiteau, R. M. and Saito, M. A.: Dynamic mercury methylation and demethylation in oligotrophic marine water, Biogeosciences, 15(21), 6451–6460, doi:10.5194/bg-15-6451-2018, 2018.

Nerentorp Mastromonaco, M. G., Gårdfeldt, K. and Wängberg, I.: Seasonal and spatial evasion of mercury from the western Mediterranean Sea, Mar. Chem., 193, 34–43, doi:10.1016/j.marchem.2017.02.003, 2017.

Nightingale, P. D., Malin, G., Law, C. S., Watson, A. J., Liss, P. S., Liddicoat, M. I., Boutin, J. and Upstill-Goddard, R. C.: In situ evaluation of air-sea gas exchange parameterizations using novel conservative and volatile tracers, Global Biogeochem. Cycles, 14(1), 373–387, doi:10.1029/1999GB900091, 2000.

Ortiz, V. L., Mason, R. P. and Evan Ward, J.: An examination of the factors influencing mercury and methylmercury particulate distributions, methylation and demethylation rates in laboratory-generated marine snow, Mar. Chem., 177, 753–762, doi:10.1016/j.marchem.2015.07.006, 2015.

555 Rimondi, V., Costagliola, P., Lattanzi, P., Morelli, G., Cara, G., Cencetti, C., Fagotti, C., Fredduzzi, A., Marchetti, G., Sconocchia, A. and Torricelli, S.: A 200 km-long mercury contamination of the Paglia and Tiber floodplain: Monitoring results and implications for environmental management, Environ. Pollut., 255, 113191, doi:10.1016/j.envpol.2019.113191, 2019.

Rosati, G., Heimbürger, L. E., Melaku Canu, D., Lagane, C., Laffont, L., Rijkenberg, M. J. A., Gerringa, L. J. A., Solidoro, C., Gencarelli, C. N., Hedgecock, I. M., De Baar, H. J. W. and Sonke, J. E.: Mercury in the Black Sea: new insights from
560 measurements and numerical modeling, Global Biogeochem. Cycles, 32(4), 1–22, doi:10.1002/2017GB005700, 2018.

Rosati, G., Solidoro, C. and Canu, D.: Mercury dynamics in a changing coastal area over industrial and postindustrial phases: Lessons from the Venice Lagoon, Sci. Total Environ., 743(July), 1–15, doi:10.1016/j.scitotenv.2020.140586, 2020.

Rosati, G., Canu, D., Lazzari, P. and Solidoro, C.: OGSTM-BFM-Hg model code. Zenodo. doi:/10.5281/zenodo.5851442, 2022.

565 Rosati, G., Laurent, C., Solidoro, C. and Canu, D.: Developing a model for mercury cycling in coastal areas. in prep.

Salon, S., Cossarini, G., Bolzon, G., Feudale, L., Lazzari, P., Teruzzi, A., Solidoro, C. and Crise, A.: Novel metrics based on biogeochemical argo data to improve the model uncertainty evaluation of the cmems mediterranean marine ecosystem forecasts, Ocean Sci., 15(4), 997–1022, doi:10.5194/os-15-997-2019, 2019.

Schaefer, J. K. and Morel, F. M. M.: High methylation rates of mercury bound to cysteine by Geobacter sulfurreducens, Nat.
570 Geosci, 2(2), 123–126, 2009.

Schartup, A. T., Ndu, U., Balcom, P. H., Mason, R. P. and Sunderland, E. M.: Contrasting effects of marine and terrestrially derived dissolved organic matter on mercury speciation and bioavailability in seawater, Environ. Sci. Technol., 49(10), 5965–5972, doi:10.1021/es506274x, 2015.

Schartup, A. T., Qureshi, A., Dassuncao, C., Thackray, C. P., Harding, G. and Sunderland, E. M.: A Model for Methylmercury
575 Uptake and Trophic Transfer by Marine Plankton, Environ. Sci. Technol., 52(2), 654–662, doi:10.1021/acs.est.7b03821, 2018.

Schlitzer, R.: Ocean Data View, [online] Available from: http://odv.awi.de, 2014.

De Simone, F., Gencarelli, C. N., Hedgecock, I. M. and Pirrone, N.: Global atmospheric cycle of mercury: a model study on the impact of oxidation mechanisms, Environ. Sci. Pollut. Res., 21(6), 4110–4123, doi:10.1007/s11356-013-2451-x, 2014.

Sonke, J. E., Heimbürger, L. E. and Dommergue, A.: Mercury biogeochemistry: Paradigm shifts, outstanding issues and
580 research needs, Comptes Rendus - Geosci., 345(5–6), 213–224, doi:10.1016/j.crte.2013.05.002, 2013.

Sunderland, E. M., Krabbenhoft, D. P., Moreau, J. W., Strode, S. A. and Landing, W. M.: Mercury sources, distribution, and bioavailability in the North Pacific Ocean: Insights from data and models, Global Biogeochem. Cycles, 23(2), 1–14, doi:10.1029/2008GB003425, 2009.

Terzić, E., Lazzari, P., Organelli, E., Solidoro, C., Salon, S., D'Ortenzio, F. and Conan, P.: Merging bio-optical data from
585 Biogeochemical-Argo floats and models in marine biogeochemistry, Biogeosciences, 16(12), 2527–2542, doi:10.5194/bg-16-2527-2019, 2019.

Tseng, C. M., Ang, S. J., Chen, Y. S., Shiao, J. C., Lamborg, C. H., He, X. and Reinfelder, J. R.: Bluefin tuna reveal global patterns of mercury pollution and bioavailability in the world's oceans, Proc. Natl. Acad. Sci. U. S. A., 118(38), 1–6, doi:10.1073/pnas.2111205118, 2021.

UNEP: Global mercury assessment 2018, Geneva, Switzerland. [online] Available from: http://www.chem.unep.ch/mercury/report/GMA-report-TOC.htm%5Cnhttp://www.chem.unep.ch/MERCURY/Report/revdraft-afterWG/assessment-report-4Oct02.pdf, 2019.

Vichi, M., Lovato, T., Lazzari, P., Cossarini, G., Gutierrez Mlot, E., Mattia, G., Masina, S., McKiver, W., Pinardi, N., Solidoro, C., Tedesco, L. and Zavatelli, M.: The Biogeochemical Flux Model (BFM) Equation Description and User Manual, , 5(August), 1–104, 2015.

Vignati, D. A. L., Burdino, E., Congiu, A. M., Cicala, F., Pardos, M., Nieddu, G. F. and Ugazio, G.: Quality evaluation of sediments from 24 tributaries of the Po River, Italy, Water. Air. Soil Pollut., 190(1–4), 129–141, doi:10.1007/s11270-007-9586-7, 2008.

Wang, K., Munson, K. M., Armstrong, D. A., Macdonald, R. W. and Wang, F.: Determining seawater mercury methylation and demethylation rates by the seawater incubation approach : A critique, Mar. Chem., 219(January), 103753, doi:10.1016/j.marchem.2020.103753, 2020.

Wu, P., Zakem, E. J., Dutkiewicz, S. and Zhang, Y.: Biomagnification of Methylmercury in a Marine Plankton Ecosystem, Environ. Sci. Technol., 54, 5446–5455, doi:10.1021/acs.est.9b06075, 2020.

Wu, P., Dutkiewicz, S., Monier, E. and Zhang, Y.: Bottom-Heavy Trophic Pyramids Impair Methylmercury Biomagnification in the Marine Plankton Ecosystems, Environ. Sci. Technol., 55(22), 15476–15483, doi:10.1021/acs.est.1c04083, 2021.

Žagar, D., Petkovšek, G., Rajar, R., Sirnik, N., Horvat, M., Voudouri, A., Kallos, G. and Četina, M.: Modelling of mercury transport and transformations in the water compartment of the Mediterranean Sea, Mar. Chem., 107(1), 64–88, doi:10.1016/j.marchem.2007.02.007, 2007.

Žagar, D., Sirnik, N., Četina, M., Horvat, M., Kotnik, J., Ogrinc, N., Hedgecock, I. M., Cinnirella, S., Pirrone, Nicola, De Simone, F. and Gencarelli, C. N.: Mercury in the Mediterranean. Part 2: Processes and mass balance, Environ. Sci. Pollut. Res., 21(6), 4081–4094, doi:10.1007/s11356-013-2055-5, 2014.

Zhang, C., Dang, H., Azam, F., Benner, R., Legendre, L., Passow, U., Polimene, L., Robinson, C., Suttle, C. A. and Jiao, N.: Evolving paradigms in biological carbon cycling in the ocean, Natl. Sci. Rev., 5(4), 481–499, doi:10.1093/nsr/nwy074, 2018.

Zhang, L., Wu, S., Zhao, L., Lu, X., Pierce, E. M. and Gu, B.: Mercury Sorption and Desorption on Organo-Mineral Particulates as a Source for Microbial Methylation, Environ. Sci. Technol., 53(5), 2426–2433, doi:10.1021/acs.est.8b06020, 2019.

Zhang, Y., Jaeglé, L. and Thompson, L.: Natural biogeochemical cycle of mercury in a global three-dimensional ocean tracer model, Global Biogeochem. Cycles, 28, 553–570, doi:10.1002/2014GB004814, 2014a.

Zhang, Y., Jaeglé, L., Thompson, L. A. and Streets, D. G.: Six centuries of changing oceanic mercury, Global Biogeochem. Cycles, 28(11), 1251–1261, doi:10.1002/2014GB004939, 2014b.

https://doi.org/10.5194/bg-2022-14
Preprint. Discussion started: 14 February 2022

Zhang, Y., Soerensen, A. L., Schartup, A. T. and Sunderland, E. M.: A global model for methylmercury formation and uptake at the base of marine food webs, Global Biogeochem. Cycles, 1–21, doi:10.1029/2019GB006348, 2020.

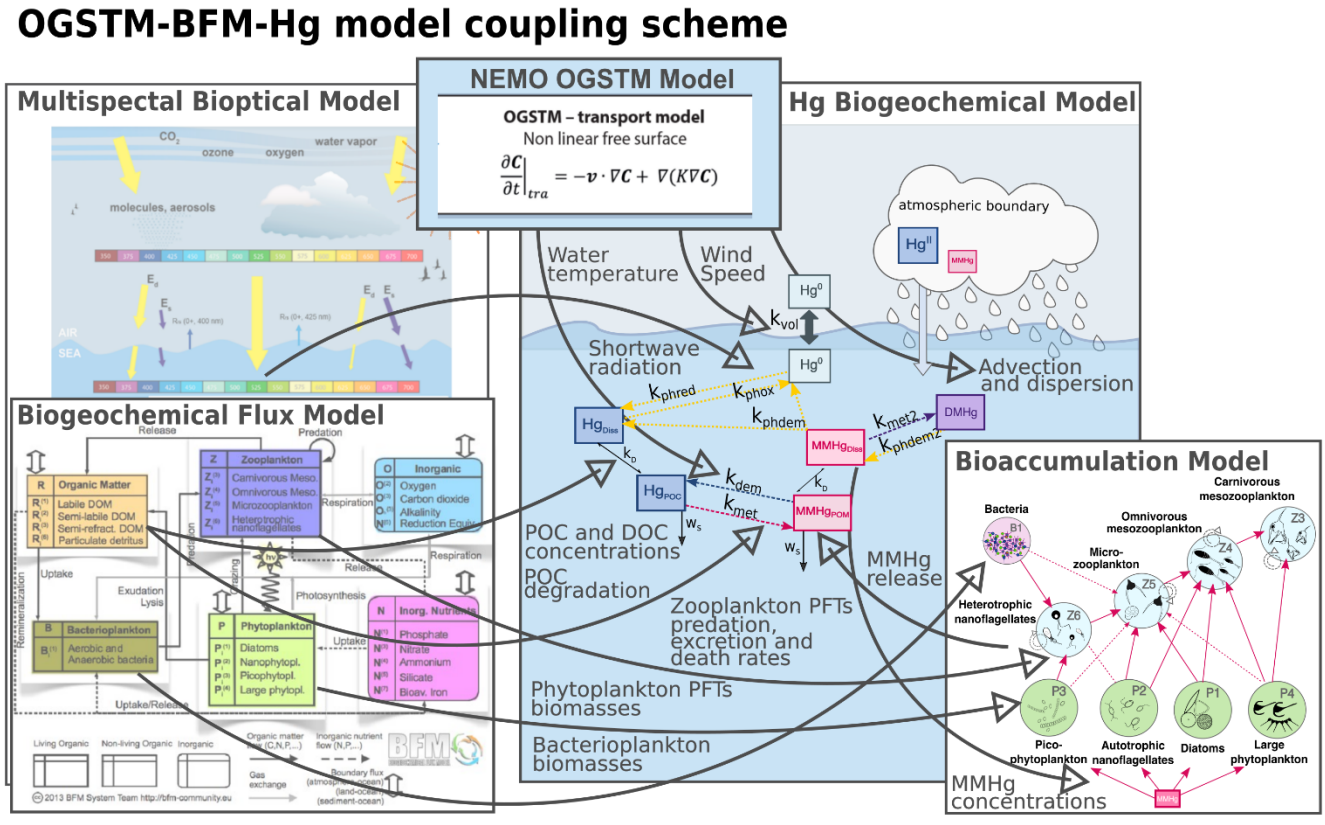

625 **Figure 1: Overview of the coupling in the OGSTM-BFM-Hg model, which integrates the biogeochemistry and bioaccumulation of Hg species in the OGSTM-BFM model, previously coupled to the transport model NEMO (Salon et al., 2019) and to a multispectral biotical model (Lazzari et al., 2021). The thick grey arrows with text highlight variables and fluxes read by the Hg biogeochemical model (Fig. 2).**

https://doi.org/10.5194/bg-2022-14
Preprint. Discussion started: 14 February 2022

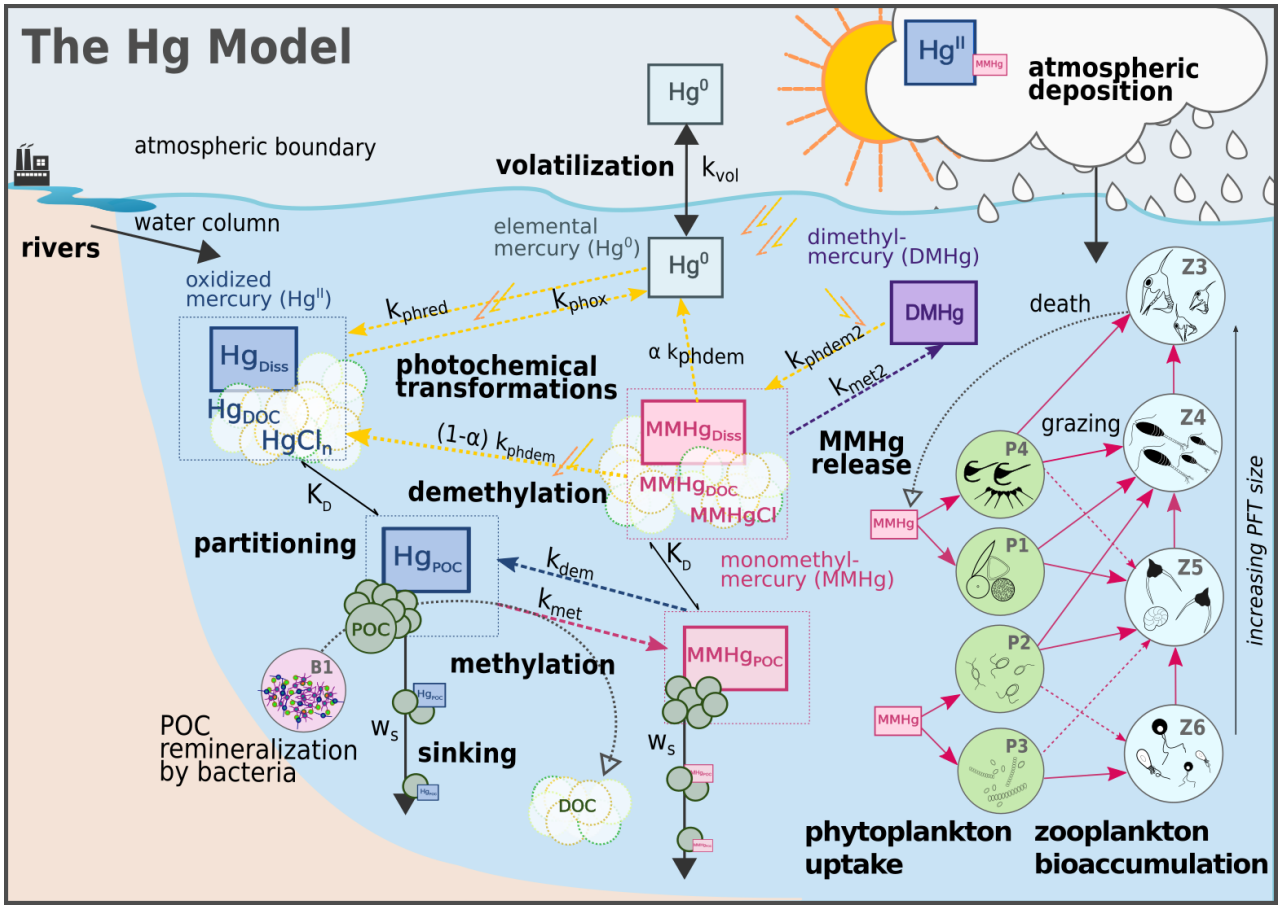

Figure 2: Hg dynamics in the coupled model OGSTM-BFM-Hg. The Hg model simulates the cycling of inorganic (Hg^{II} and Hg^0) and methylated Hg species (MMHg and DMHg) resolving: the partitioning of Hg^{II} and MMHg between particulate (Hg_{POC}, $MMHg_{POC}$) and dissolved species (Hg_{Diss}, as Hg_{DOC} + HgCln, and $MMHg_{Diss}$, as $MMHg_{DOC}$ + MMHgCl) based on partition coefficients (K_D) and concentrations of POC and DOC, the photochemical and biological transformations (dotted colored arrows) as first order kinetics depending on the rate constants k_x, the evasion of Hg^0 to the atmosphere controlled by wind speed through the volatilization rate constant k_{vol}, and the MMHg bioaccumulation (pink arrows) driven by phytoplankton uptake in 4 different PFTs and trophic transfer to 4 zooplankton PFTs.

https://doi.org/10.5194/bg-2022-14
Preprint. Discussion started: 14 February 2022

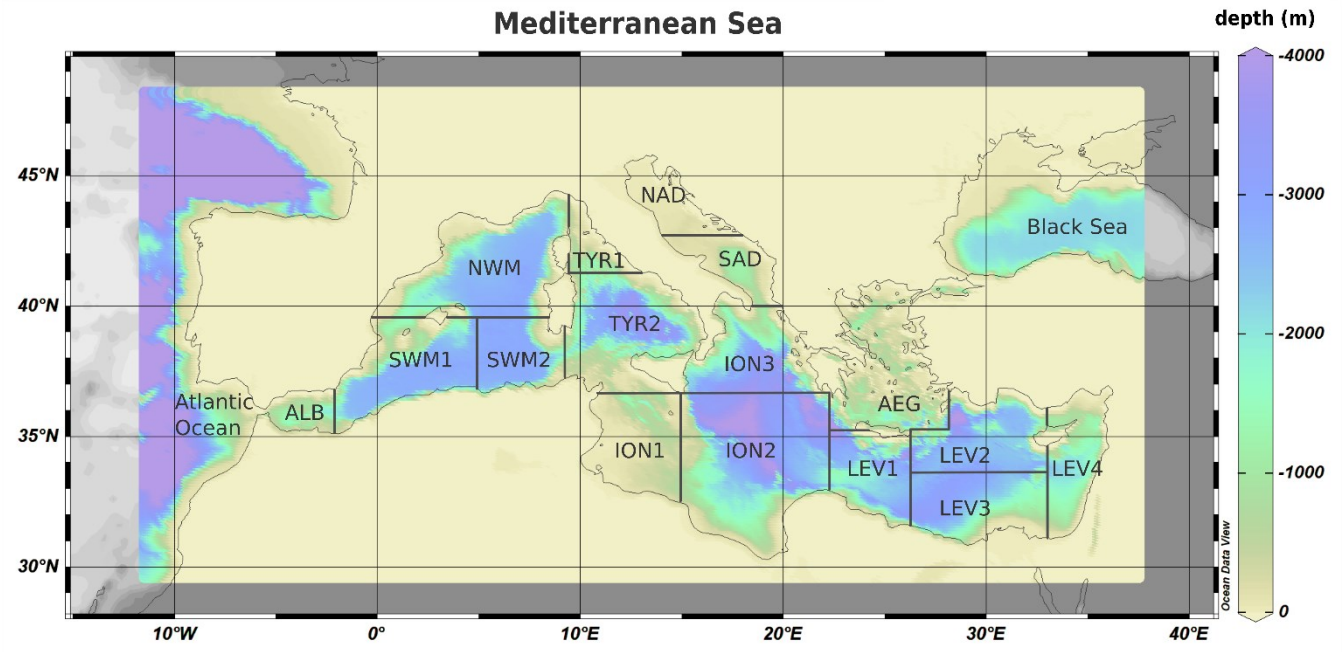

Figure 3: Bathymetric map of the Mediterranean Sea showing the subdivision of the model domain in subbasins: Alboran Sea (ALB), southwest western Mediterranean (SWM1 and SWM2), northwestern Mediterranean (NWM), Tyrrhenian Sea (TYR1 and TYR2), northern Adriatic Sea (NAD), southern Adriatic Sea (SAD), Ionian Sea (ION1, ION2, and ION3), Aegean Sea (AEG), and Levantine basin (LEV1, LEV2, LEV3, and LEV4). The bathymetric map is from Ocean Data View (Schlitzer, 2014).

https://doi.org/10.5194/bg-2022-14
Preprint. Discussion started: 14 February 2022

Biogeosciences Discussions Open Access EGU

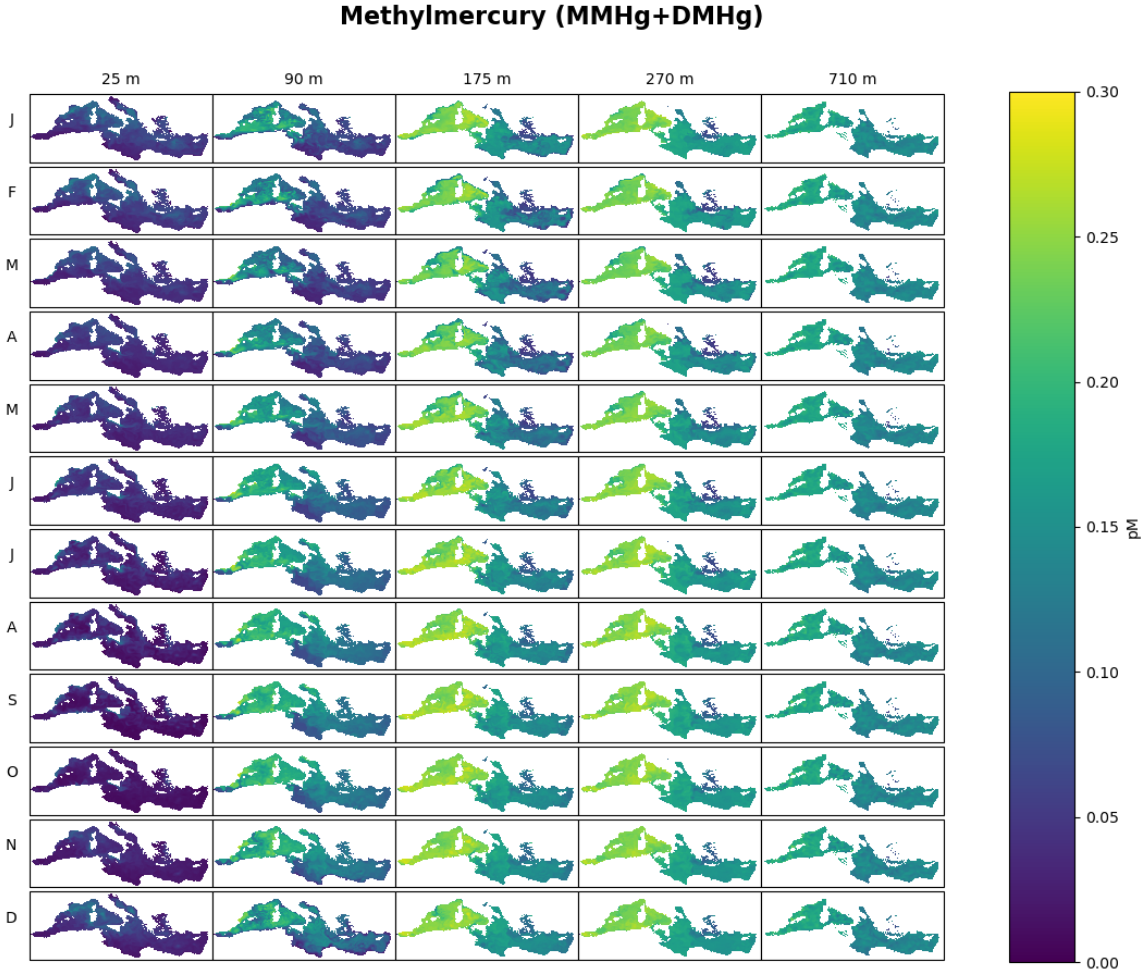

Figure 4: Spatial distribution of monthly averaged MeHg concentrations (pM) in the Mediterranean Sea at different depths in the water column (25, 90, 175, 270 and 710 m-depth) simulated with the OGSTM-BFM-Hg model.

https://doi.org/10.5194/bg-2022-14
Preprint. Discussion started: 14 February 2022

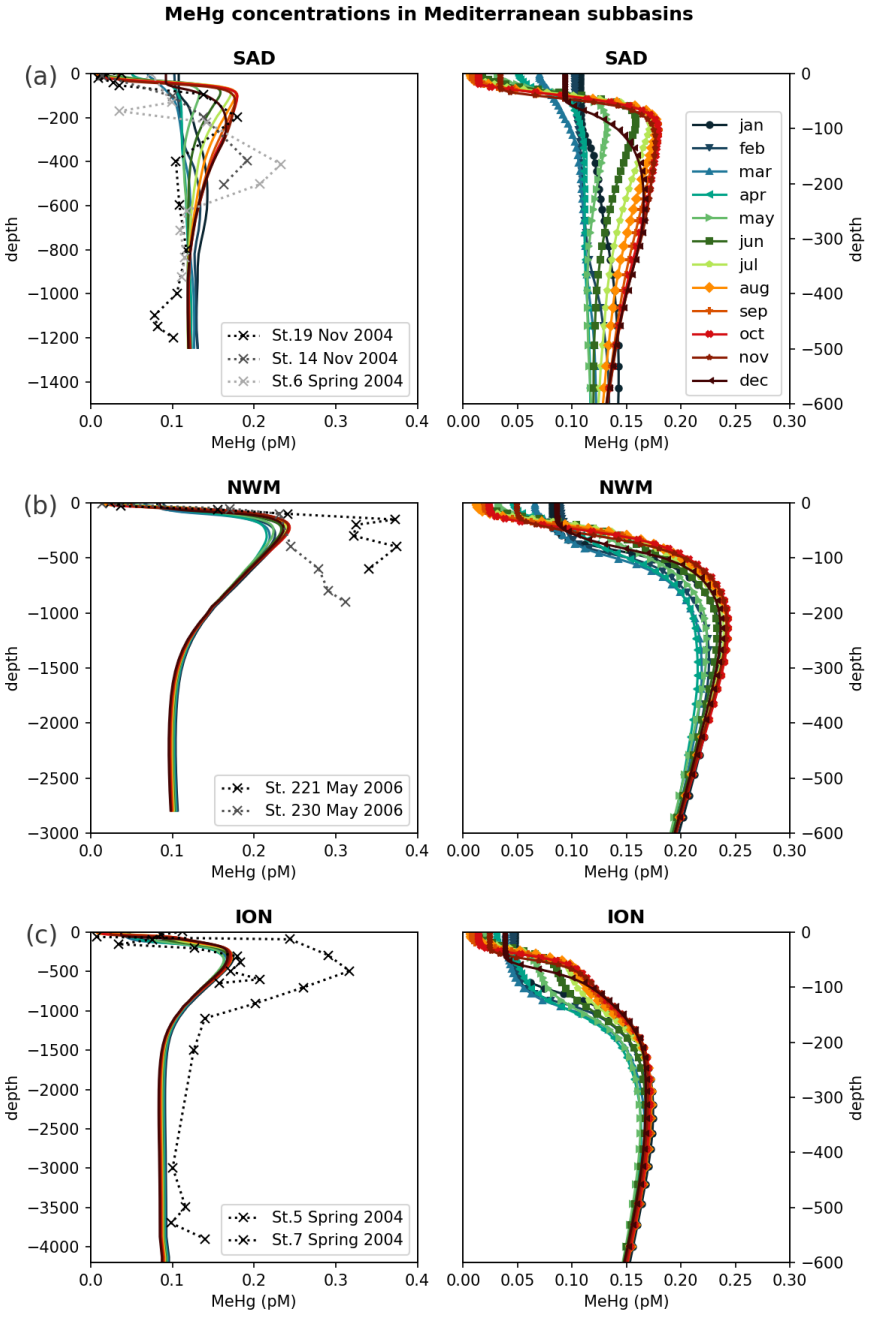

Figure 5: Vertical profiles of monthly averaged MeHg (MMHg+DMHg) concentrations in the water column reproduced by OGSTM-BFM-Hg model for 2017 (colored solid lines), compared with observations for 2004-2005 (dotted lines with crosses) available from the literature (Cossa et al., 2009) in three subbasins (Fig. 3): (a) Southern Adriatic Sea (SAD), (b) North Western Mediterranean (NWM), and (c) Ionian Sea (ION2). The right panels show the entire water column and the left panels show a detail of modelled concentrations in the top 600 m of the same subbasins.

https://doi.org/10.5194/bg-2022-14
Preprint. Discussion started: 14 February 2022

Biogeosciences
Discussions
Open Access
EGU

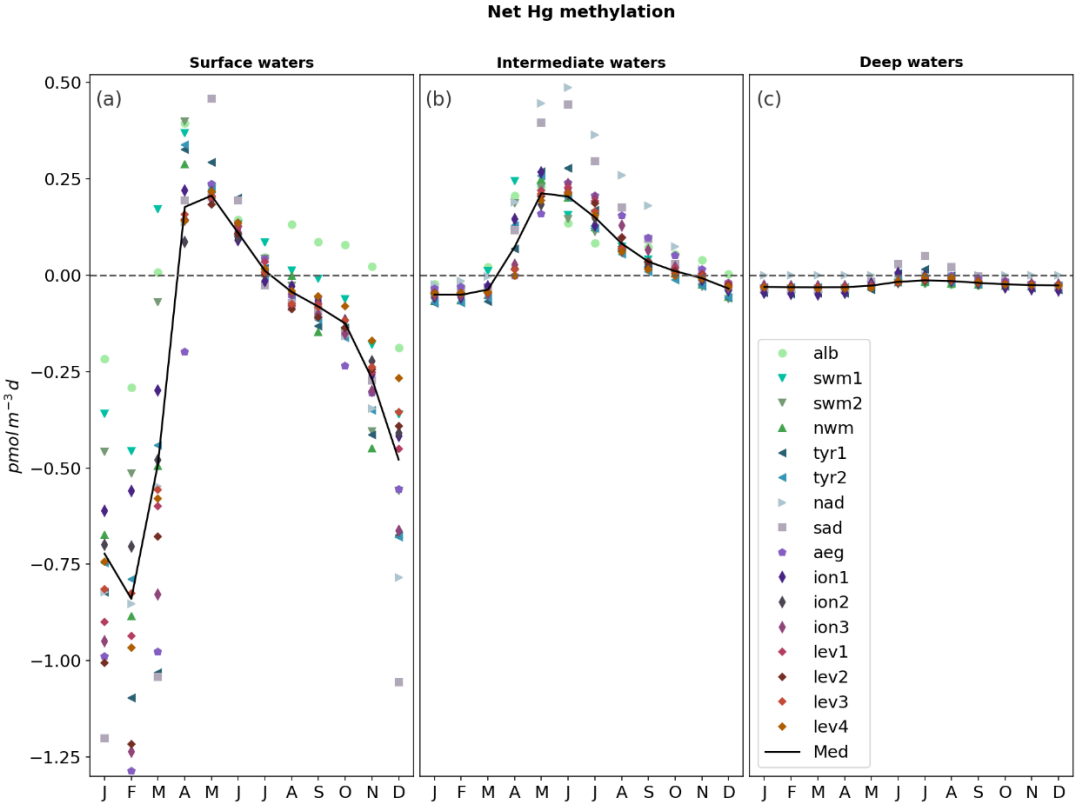

Figure 6: Monthly evolution of the net methylation fluxes (pmol m^{-3} d^{-1}) for each subbasin (colored markers) of the Mediterranean Sea (black lines) depth-integrated for (a) surface water (0-100 m depth), (b) intermediate water (100-600 m depth), and (c) deep water (>600 m depth). Net methylation is calculated as the difference between modelled Hg methylation fluxes and demethylation fluxes (both dark and photochemical).

https://doi.org/10.5194/bg-2022-14
Preprint. Discussion started: 14 February 2022

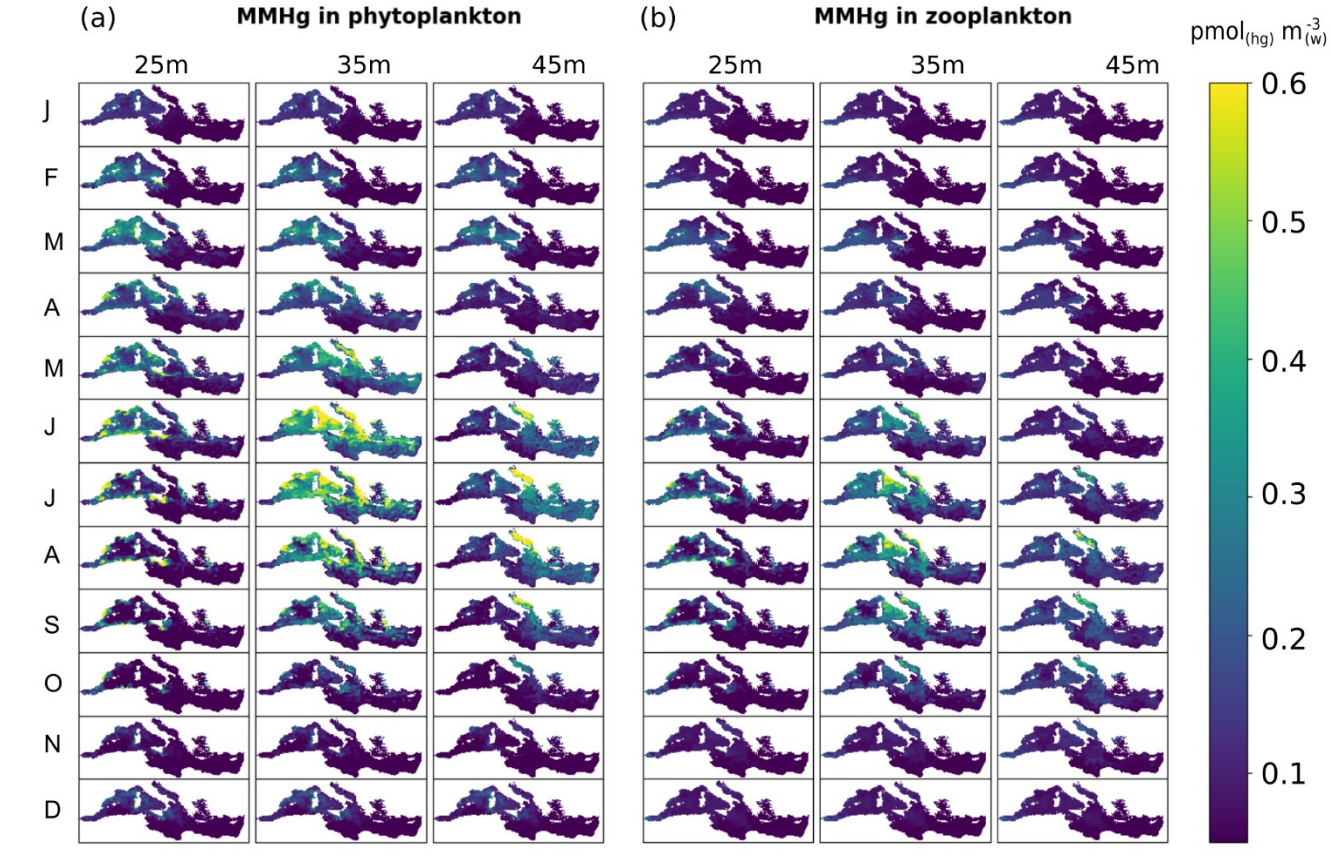

Figure 7: Spatial distribution of monthly averaged (a) $MMHg_{phy}$ and (b) $MMHg_{zoo}$ ($pmol_{(hg)}$ $m_{(w)}^{-3}$) in the Mediterranean Sea at different water depths (25 m, 35 m, and 45 m) simulated with the OGSTM-BFM-Hg model for 2017. The plots show the sum of all variables of MMHg in phytoplankton (Fig. S7-S10) and zooplankton (Fig. S11-S14).

https://doi.org/10.5194/bg-2022-14
Preprint. Discussion started: 14 February 2022

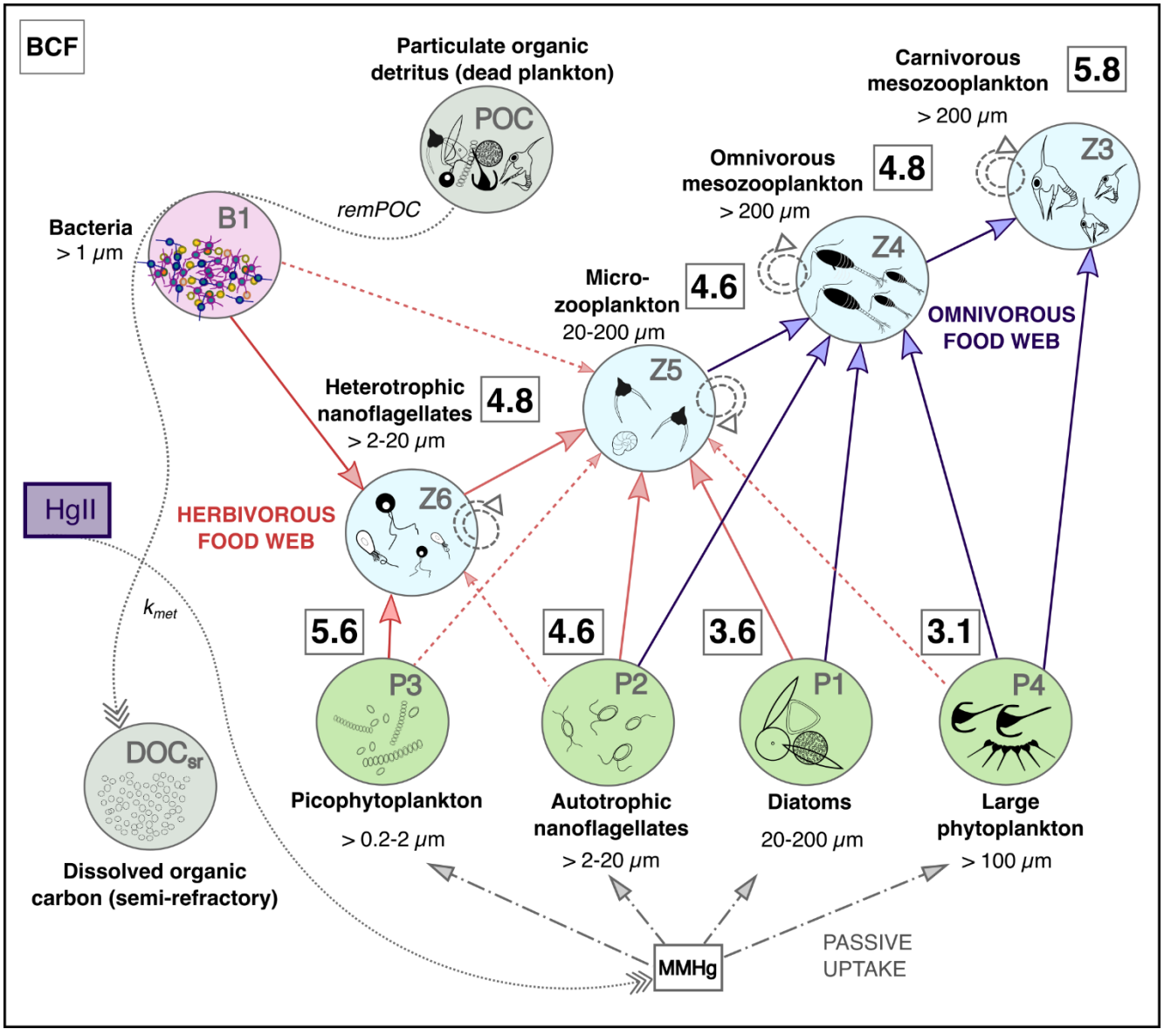

Figure 8. Conceptual model of MMHg bioaccumulation in the plankton food web of the SAD subbasin of the OGSTM-BFM-Hg model, subdivided into a lower "herbivorous" (red arrows) and upper "omnivorous" (blue arrows) food webs. The solid arrows show the preferential trophic interactions, the dashed arrows are for secondary trophic interactions (diet switch if the favorite preys are not available), and the circle dashed arrows are for cannibalization within the same zooplankton group. The dash and dotted arrows indicate passive uptake of MMHg by phytoplankton. The dotted arrows indicate the processes of transformation related to carbon recycling by bacteria (remPOC) and of Hg methylation, whose kinetics are coupled through the parameter k_{met}, converting Hg^{II} into MMHg. The squares with bold numbers show estimated values of BCF (Bioconcentration factors, log(kg l^{-1})) for each PFT, calculated from spatially averaged model output at monthly resolution. The green circles indicate the four phytoplankton PFTs (P1, P2, P3, P4, representative respectively of diatoms, autotrophic nanoflagellates, picophytoplankton and large phytoplankton), the light blue circles indicate the four zooplankton PFTs (Z3, Z4, Z5, Z6, representative respectively of carnivorous mesozooplankton, omnivorous mesozooplankton, microzooplankton, and heterotrophic nanoflagellates), the purple circle indicate bacteria (B1, representative of all heterotrophic bacteria), and the grey circles indicate particulate organic carbon (POC, representative of all organic detritus) and semi-refractory dissolved organic matter (DOC_{sr}).

https://doi.org/10.5194/bg-2022-14
Preprint. Discussion started: 14 February 2022

Biogeosciences Discussions Open Access EGU

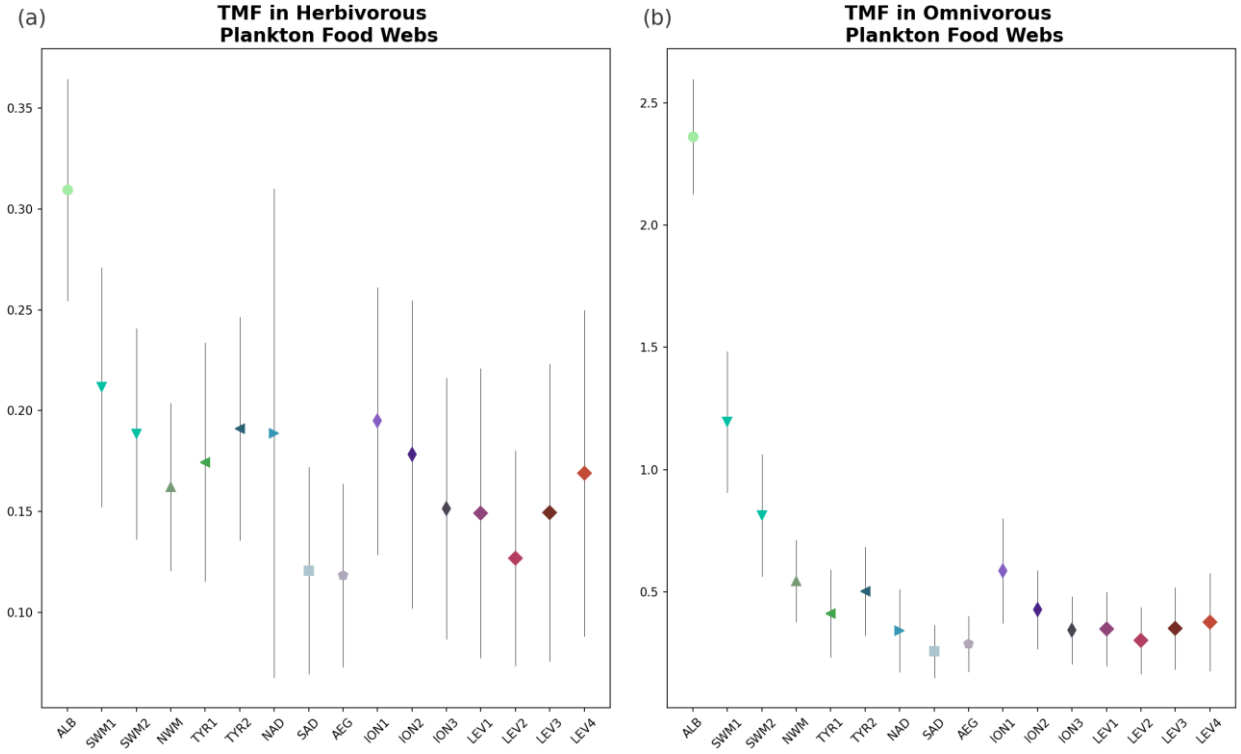

680

Figure 9. Trophic magnification factor (TMF, unitless) for the (a) onmivorous and (b) carnivorous plankton food webs (Figure 8) for each subbasin of the Mediterranean Sea (Figure 3), calculated by integrating over 0-100 m depth the monthly outputs of the OGSTM-BFM-Hg model.

685

https://doi.org/10.5194/bg-2022-14
Preprint. Discussion started: 14 February 2022

		***Phytoplankton* PFTs**			
		Diatoms	**Autotrophic Nanoflagellates**	**Pico-phytoplankton**	**Large phytoplankton**
$MMHg_{phy,\,PFT}$	*ALB*	**7.1 10^{-4}** (± 5.9 10^{-4})	**5.1 10^{-3}** (± 3.5 10^{-3})	**0.09** (±0.05)	**1.5 10^{-5}** (± 8.8 10^{-6})
	SAD	**1.5 10^{-3}** (± 2.7 10^{-3})	**2.6 10^{-3}** (± 3.3 10^{-3})	**0.14** (±0.16)	**5.1 10^{-7}** (± 6.4 10^{-7})
$Q_{MMHg,PFT}$	*ALB*	**0.02** (± 0.01)	**0.15** (± 0.09)	**1.57** (± 1.01)	**5.9 10^{-3}** (± 3.7 10^{-3})
	SAD	**0.03** (± 0.02)	**0.27** (± 0.22)	**2.80** (± 2.22)	**8.9 10^{-3}** (± 7.2 10^{-3})
$BCF_{phy,PFT}$	*ALB*	**3.59** (± 0.08)	**4.58** (± 0.08)	**5.59** (± 0.07)	**3.17** (± 0.08)
	SAD	**3.59** (± 0.1)	**4.60** (± 0.08)	**5.60** (± 0.07)	**3.14** (± 0.07)
		Zooplankton PFTs			
		Heterotrophic Nanoflagellates	**Micro-zooplankton**	**Onmivorous mesozooplankton**	**Carnivorous mesozooplankton**
$MMHg_{zoo,\,PFT}$	*ALB*	**9.1 10^{-2}** (± 2.9 10^{-2})	**2.6 10^{-2}** (± 5.1 10^{-3})	**2.1 10^{-3}** (± 5.4 10^{-3})	**1.9 10^{-2}** (± 1.6 10^{-3})
	SAD	**7.2 10^{-2}** (± 7.9 10^{-2})	**1.6 10^{-2}** (± 1.7 10^{-2})	**7.1 10^{-3}** (± 7.1 10^{-3})	**1.0 10^{-3}** (± 2.7 10^{-4})
$Q_{MMHg,\,PFT}$	*ALB*	**0.39** (±0.34)	**0.31** (±0.29)	**0.35** (±0.36)	**1.04** (±0.2)
	SAD	**0.73** (±0.83)	**0.42** (± 0.55)	**0.79** (±1.2)	**3.60** (±2.2)
$BCF_{zoo,PFT}$	*ALB*	**4.90** (± 0.17)	**4.78** (± 0.24)	**4.86** (± 0.21)	**5.50** (± 0.29)
	SAD	**4.80** (± 0.36)	**4.58** (± 0.40)	**4.79** (± 0.53)	**5.81** (± 0.36)

690 **Table 1: Indicators for MMHg bioaccumulation compared for the ALB and SAD subbasins (Fig. 3). The average (± s.d.) values of the plankton MMHg content ($MMHg_{PFT}$, pmol m^{-3}), the MMHg quota ($Q_{MMHg,PFT,}$ ng $g_{w.w.}^{-1}$), and the bioconcentration factors (BCF, log[l kg^{-1}]) are shown for each phytoplankton and zooplankton PFT.**